# Implementation of a new crop phenology and irrigation scheme in the ISBA land surface model using SURFEX_v8.1

Arsène Druel[1,2], Simon Munier[1], Anthony Mucia[1], Clément Albergel[1,3] and Jean-Christophe Calvet[1]

[1]CNRM, Université de Toulouse, Météo-France, CNRS, Toulouse, France
5 [2]Now at Ecologie des Forêts Méditerranéennes (URFM), Institut national de recherche pour l'agriculture, l'alimentation et l'environnement (INRAE), Avignon, France
[3]Now at European Space Agency Climate Office, ECSAT, Harwell Campus, OX11 0FD Didcot, Oxfordshire, United Kingdom

*Correspondence to*: Jean-Christophe Calvet (jean-christophe.calvet@meteo.fr), Arsène Druel
10 (arsene.druel@umr-cnrm.fr)

**Abstract.** With an increase in the number of natural processes represented, global land surface models (LSMs) have become more and more accurate in representing natural terrestrial ecosystems. However, they are still limited with respect to the impact of agriculture on land surface variables. This is particularly true for agro-hydrological processes related to a strong human control on freshwater. While 15 most LSMs consider natural processes only, the development of human-related processes, e.g. crop phenology and irrigation in LSMs, is key. In this study we present the implementation of a new crop phenology and irrigation scheme in the ISBA (Interaction between Soil, Biosphere, and Atmosphere) LSM. This highly flexible scheme is designed to account for various configurations and can be applied at different spatial scales. For each vegetation type within a model grid cell, three irrigation systems can 20 be used at the same time. A limited number of parameters are used to control (1) the amount of water used for irrigation, (2) irrigation triggering (based on the soil moisture stress) and (3) crop seasonality (emergence, harvesting). A case study is presented over Nebraska (USA). This region is chosen for its high irrigation density and because independent observations of irrigation practices can be used to verify the simulated irrigation amounts. The ISBA simulations with and without the new crop 25 phenology and irrigation scheme are compared to different satellite-based observations. The comparison shows that the irrigation scheme improves the simulated vegetation variables such as leaf area index, gross primary productivity, and land surface temperature. In addition to a better representation of land

surface processes, the results point to potential applications of this new version of the ISBA model for water resource monitoring and climate change impact studies.

## 1 Introduction

Amongst the global water withdrawal from rivers, reservoirs and groundwater, the share used for agriculture is estimated to reach 69 % on average, with some regional heterogeneity - over 90 % in some regions (Hoekstra and Mekonnen, 2012, FAO, 2014). This amount of water is likely to increase in the future in relation to climate warming and population growth (United Nations et al., 2019, Field et al., 2014). The historical evolution of irrigation also points to increasing water consumption: the area equipped for irrigation nearly doubled from 1900 to 1950, when it tripled from 1950 to 2005 (Siebert et al., 2015).

Irrigation is used to increase crop yields by mitigating the soil water stress (Fraiture et al., 2007). Several studies indicate that yields can be higher by a factor of two or more when the fields are irrigated (Bruinsma, 2009; Colaizzi et al., 2009; Siebert and Döll, 2010; FAO, 2014). However, freshwater is already a limited resource and the current evolution of irrigation has a substantial impact on: (1) river discharge, with a decrease in their lower reaches due to diversions and impoundments for irrigation (Tang et al., 2008; Piao et al., 2010; Grafton et al., 2018), (2) groundwater level, with critical low levels observed in case of intensive irrigation (Rodell et al., 2009; Döll et al., 2012; Pfeiffer and Lin, 2014), (3) the surface energy budget through an increase of evapotranspiration, which can lead to surface cooling (Kueppers et al., 2007; Lobell et al., 2008; Jiang et al., 2014; de Vrese et al., 2016). Water vapour originating from large scale irrigation water supply can be recycled to rainfall (Moore and Rojstaczer, 2002; DeAngelis et al., 2010; Carrillo-Guerrero et al., 2013; Harding et al., 2013). It can also affect the dynamics of the monsoon (Douglas et al., 2006; Saeed et al., 2009; Shukla et al., 2014) and influence climate at both regional and global scales (Sacks et al., 2009; Puma and Cook, 2010). These findings show a gradual and significant influence of changes in irrigated areas on the hydrological cycle (e.g. Adegoke et al., 2003; Haddeland et al., 2006; Rost et al., 2008; Döll et al., 2009; Hanasaki et al., 2010; Biemans et al., 2011). The ability of numerical models to reproduce these

different impacts and feedbacks is thus essential in order to understand the role of irrigation in the Earth

55   climate system at different spatial scales (Zaitchik et al., 2005). Representing irrigation could potentially improve weather and climate forecast skill (Ozdogan et al., 2010). However, as presented below, irrigation is generally represented in models in a too simplistic way.

Land surface models (LSMs) provide lower boundary conditions to climate and weather forecast atmospheric models. The new generation of LSMs is able to represent land surface biophysical

60   processes and variables, including soil moisture and vegetation biomass, in a way that is fully consistent with the representation of carbon, water and energy fluxes. LSMs differ from crop models in the sense that they do not explicitly represent all the agricultural practices, nor crop yields. While most crop models have implemented irrigation, irrigation is not represented by all LSMs.However, cCurrent LSMsmodels have to improve the representation of anthropogenic factors and their interactions with

65   natural processes (Verburg et al., 2016). In particular, LSMs need to represent the complexity of irrigation practices as much as possible, and their impact on the atmosphere and on the environment. For example, efforts are made to achieve this goal in the Community Land Model (CLM), in Noah-MP, in Accelerated Climate Modeling for Energy (ACME), and in ORganizing Carbon and Hydrology in Dynamic EcosystEms (ORCHIDEE) LSMs (Felfelani et al. 2020, Zhang et al. 2020, Leng et al. 2017,

70   and Yin et al. 2020, respectively). However, aAs highlighted by Chukalla et al. (2015), a number of large scale LSMs currently represent only one type of irrigated vegetation (mostly C4 crops, i.e. crops with a C4 photosynthesis carbon fixation type, such as corn, sorghum), with only one type of irrigation practice (e.g. sprinkling or flooding), one season per year and no inter-annual variability of vegetation density (Perry, 2007; Perry et al., 2009). Among others, this is the case in the current version of the

75   ISBA (Interaction between Soil, Biosphere, and Atmosphere; Noilhan and Planton, 1989) LSM, with C4 crops irrigated with sprinkling (Voirin-Morel, 2003; Calvet et al., 2008). In reality, there are a lot of different vegetation types which can be irrigated, from orchards to pastures (FAO, 2014), and different irrigation techniques with different ways to apply water (above the vegetation or directly on the ground for sprinkling and flooding irrigation techniques, respectively). Different irrigation types vary in (1)

80   irrigation efficiency (Evans and Sadler, 2008; Jägermeyr et al., 2015), (2) the amount of freshwater used

for irrigation per surface unit (FAO, 2014), and (3) impact on water resources (Khan and Abbas, 2007). Moreover, some specificities of irrigation such as the timing and frequency of water application can affect the ecosystem and atmospheric responses to irrigation (Sorooshian et al., 2012). Some models include a representation of irrigation without having an interactive vegetation scheme and using climatological values instead (such as with the LIS-Noah model, a NASA land information system and LSM combination, used in Lawston et al., 2015), thereby precluding inter-annual variability of vegetation density and the impact of irrigation on vegetation growth. Having a more complete irrigation description is needed to reproduce the irrigation seasonality, and to represent possible changes in crop phenology such as emergence and harvest dates. The impact of changing irrigation characteristics in a context of climate change could thereby be evaluated, such as increasing irrigation efficiency (currently around 56%; FAO, 2014) and freshwater saving potential (Perry et al., 2017; Koech and Langat, 2018).

The objective of this work is to develop and evaluate a more detailed representation of crop phenology and irrigation practices into the ISBA LSM within the SURFEX (SURFace EXternalisée) modelling platform (Masson et al., 2013). The new scheme is designed to work on a global scale. We focus on a densely irrigated area in Nebraska where validation data are available.

Section 2 presents a description of the ISBA LSM, the new crop phenology and irrigation scheme, the validation protocol, followed by a description of the observational datasets. Section 3 illustrates the impact of the new scheme when compared to simulations without crop phenology and without irrigation. An evaluation of the performance of the model is made over Nebraska. Section 4 discusses the added value and the limits of the newly implemented irrigation scheme. Finally, Section 5 presents the conclusions and future research directions.

## 2 Materials and Methods

### 2.1 The ISBA land surface model

The ISBA model (originally described in Noilhan and Planton, 1989) is a LSM developed by the research department of Météo-France (Centre National de Recherches Météorologiques, CNRM). It is embedded into the SURFEX modelling platform (Masson et al., 2013; Voldoire et al., 2017; Le Moigne

et al., 2018), and can provide initial land surface conditions to various atmospheric models (e.g. ALADIN in Fischer et al., 2005), or be driven by atmospheric conditions in offline (i.e. stand-alone) mode. SURFEX integrates different models describing ocean and terrestrial surfaces. Over land, specific models are used to represent water bodies, cities, and the soil-plant system. The latter is modelled by the ISBA LSM. The ISBA model can be coupled to the CTRIP model (Decharme et al., 2019, Munier and Decharme, 2021) which is specifically designed to represent water dynamics within rivers and aquifers. Only offline ISBA simulations are considered in this study.

## 2.2 Crop phenology and irrigation modelling concept

An old irrigation scheme working at a local scale (Calvet et al., 2008) is available in the ISBA LSM. Major limitations of the old scheme are the lack of (1) spatialization on a global scale, (2) representation of harvest, (3) diversity of irrigation types and irrigated vegetation types, (4) interoperability with the multi-layer soil hydrology scheme. Key processes implemented in this scheme are briefly described below. The irrigation can be activated for ISBA versions able to simulate photosynthesis, interactive vegetation biomass and LAI (ISBA-A-gs; Calvet et al., 1998; Gibelin et al., 2006). Sprinkler irrigation is represented by imposing an additional water flux forcing to the soil-plant system. Water is applied at a given time and over a certain period of time. A number of irrigation parameters need to be assigned such as the irrigation amount, the irrigation interval, the irrigation start and end times. A parsimonious approach is used in order to limit the number of parameters of the model. Table 1 lists the parameters and the values used by default in the model. Using these values allows the model to predict a realistic amount of irrigation water over irrigated corn in southern France (Bonnemort et al., 1996; Voirin-Morel, 2003; Calvet et al., 2008). Irrigation is triggered using thresholds of the simulated extractable soil moisture content, when vegetation growth is limited by a soil moisture deficit. The plant water stress level is evaluated using a unitless soil wetness index along the root profile ($SWI_{root\_zone}$). A $SWI_{root\_zone}$ value close to one corresponds to a well-watered soil, while a value close to zero indicates extreme stress. In order to trigger irrigation, the $SWI_{root\_zone}$ value is compared to predefined SWI thresholds given as input parameters. These SWI thresholds are evolving during the irrigation season and default values are fixed to 0.7 for the first irrigation, 0.55 for the second

irrigation, 0.4 for the third irrigation, and 0.25 afterwards. The use of these values was validated by
Bonnemort et al. (1996), Voirin-Morel (2003) and Calvet et al. (2008). The idea behind this approach is
that irrigation does not completely refill the soil, especially at the end of the growing season.
Mechanical harvest requires relatively dry conditions to avoid soil compaction. The crop is allowed to
use rainwater together with the initial available water content of the soil. This irrigation strategy allows
the optimization of water withdrawal according to plant water extracting abilities at different crop
growing stages. When a SWI threshold is reached, irrigation is triggered with a predefined quantity of
water of 30 mm (by default), following Calvet et al. (2008).

### 2.2.1 New crop phenology processes

In this study, ISBA-A-gs is used together with the multi-layer soil hydrology scheme described in
Decharme et al. (2019). In ISBA-A-gs, phenology is entirely driven by photosynthesis and no growing
degree-day model is used. The only phenology parameter is a minimum LAI value, of 0.3 $m^2m^{-2}$ for low
vegetation. In the new scheme, specific crop phenology parameters such as emergence and harvest dates
are used for irrigated crops. In practice, two dates are prescribed: emergence and harvest. This is a
simple way to represent specific crop phenology attributes of irrigated crops. Between these two dates,
irrigation is possible. Before the emergence and after the harvest, LAI is fixed at the model's minimum
value (LAI = 0.3 $m^2$ $m^{-2}$). The new scheme provides the option to support up to three plant growth
seasons per year. The crop phenology parameters are not applied to wooded vegetation (trees and
shrubs), and can be applied without irrigation.

### 2.2.2 New irrigation processes

In the new scheme, three irrigation types are considered: sprinkler irrigation, flood irrigation and drip
irrigation. The same irrigation types as in Lawston et al. (2015) are represented but a different
modelling approach is used.

For sprinkler irrigation settings, Tthe irrigation water flux is evenly distributed over a period of
time of 8 hours (by default) and is applied on top of the vegetation canopy like precipitation. The

irrigation water can be intercepted by vegetation canopy. The new irrigation algorithm is based on several steps described below and in Fig. 1.

Firstly, the model determines whether fields within the grid cell can be irrigated, i.e. they are equipped for irrigation (e.g. water supply, valves, pipes…). This information is given by the irrigation map described in section 2.4.1.

Secondly, the model checks whether the vegetation growth stage is compatible with irrigation. For crops, irrigation can be triggered after the emergence and until a few days before the harvest (by default two weeks).

The availability of resources (equipment or local water distribution) is taken into account through a default minimum time gap between two successive irrigations (Zhang et al. 2019). This default irrigation interval parameter value is a constant (7 days by default) but maps of irrigation intervals could be used when available.

Since a multi-layer soil hydrology scheme is used in the new irrigation model, the root-zone SWI ($SWI_{root\_zone}$) is a weighted average SWI value based on the soil volumetric water content profile ($Wc_i$, m$^3$ m$^{-3}$), the field capacity volumetric water content profile ($Wfc_i$, m$^3$ m$^{-3}$) and the wilting point profile ($Wwilt_i$, depending on clay and sand fraction, m$^3$ m$^{-3}$), for each soil layer $i$. The root fraction inside each soil layer ($f_{root_i}$) is used as a weighting factor:

$$SWI_{root\_zone} = \sum_{i=1}^{n_{soil}} f_{root_i} \times \frac{Wc_i - Wwilt_i}{Wfc_i - Wwilt_i} \tag{1}$$

where $n_{soil}$ is the total number of soil layers in the root zone. This value depends on the considered vegetation type. For example, $n_{soil} = 9$ for crops, with a rooting depth of 1.5 m.

In addition to sprinkler irrigation, the new model is able to represent drip or flood irrigation. In this case, the water flux is applied directly to the soil surface, without leaf interception. Considering the static equipment used for drip irrigation, there is no irrigation interval ($\Delta t_{Wn} = 0$ day). In this study, only sprinkling irrigation is considered as this is the dominant irrigation type in Nebraska. Drip and flood irrigation will be evaluated in future works. The activation of a given irrigation method is described in Supplement S5. Irrigation simulations are illustrated in Supplements S2 and S3 over southwestern France and over the Hampton irrigated area in Nebraska (Fig. 2e and Figs. S2~~1.2~~ and S3~~1.3~~),

respectively. Observed monthly precipitation in Nebraska is presented for contrasting years in Supplement S4.

All the values of the model parameters in Table 1 have been set within a default configuration.
These values can be user-defined for each "~~nature~~land surface type" and for each grid cell, including,
190 when possible, seasonal variations. See Supplement S5 for configuration details and possibilities.

### 2.2.3 New aggregation rules of irrigated and rainfed vegetation

The new crop phenology and irrigation scheme is operated using ECOCLIMAP-SG to prescribe land cover (Calvet and Champeaux, 2000 ; Supplement S1). The best achievable spatial resolution of ECOCLIMAP-SG is 300 m × 300 m. In contrast to previous versions of ISBA, there is no specific
195 irrigated ~~nature~~ land surface type in the new ECOCLIMAP-SG vegetation description. On the other hand, irrigation of all the twenty land surface ~~nature~~ types listed in Fig. S1.~~1~~ and Table S2~~1.2~~ is possible. By default, six vegetation types are considered: ~~(~~three crop and three woody vegetation types ~~as shown in~~ (Fig. S1.~~1~~). The new scheme is able to represent the sub-grid heterogeneity of the irrigation fractional coverage. For example, ~~This is illustrated over North America by Figs. S1.2 and S1.3,~~
200 ~~showing~~ distinct maps of the fraction of irrigated C4 and C3 crops can be produced over North America (Figs. S2 and S3, respectively). For each land surface ~~nature~~ type, an irrigated and a non-irrigated fraction are considered at the simulation resolution. In order to prevent an excessive increase in the number of simulated land surface ~~nature~~ types (potentially 20 non-irrigated and 20 irrigated times 3 irrigation types, i.e. a total of ~~120~~80 types), involving a large increase of complexity, memory and
205 computing cost, some choices are made for the implementation:

1. Selection of a limited number of irrigated land surface ~~nature~~ types. The default implementation consists in six irrigated land surface ~~nature~~ types. Temperate deciduous and evergreen trees types (No 8 and 10 in Table S2~~1.2~~, respectively) can be used to represent fruits trees or olive trees for example, respectively. Shrub type (No 15) can be used to
210 represent, among others, vine plants, and types No 19, 20 and 21 may represent irrigated crops (e.g. wheat, soybean, and corn, respectively).

2. Selection of the main irrigation method used for each grid cell and land surface ~~nature~~ type, considering that in one grid cell there is only one dominant method for a given land surface ~~nature~~ type (e.g. flooded rice in China or sprinkled corn in France).

215 Finally, the system state variables (soil water content, surface and soil temperature, vegetation biomass, etc.) differ in irrigated and non-irrigated parts of the cell. This implies to (1) duplicate a land surface ~~nature~~ type if it is partially irrigated, (2) attribute for each grid cell the corresponding irrigated fraction, and (3) select the irrigation type for the irrigated fraction. Lastly, the two irrigated and non-irrigated land surface ~~nature~~ types are treated separately but the same rooting depth and secondary

220 parameters (see Table S1.~~1~~) are used.

In order to limit the computing time, vegetation types can (optionally) be gathered. In this case vegetation "patches" are created (see Supplement S1 and Fig. S4~~1.4~~). Firstly, irrigated land surface types are duplicated in order to ensure the distinction of irrigated and rainfed soil water budgets. Patch aggregation rules are then used to merge the land surface types. Finally, model parameter values are

225 computed following the new patch fraction map.

## 2.3 Experimental design

The simulations and the evaluation of the new scheme are made over the state of Nebraska (United States of America, USA). This area presents a high density of irrigated fields (Fig. 2) and large freely available observational datasets for evaluation. In this area, most irrigated field consist of corn (Zhang

230 et al., 2020). In particular, we focus on a region where the irrigation is prominent: the south of the state of Nebraska (100-97°W, 40.25-41.25°N, Fig. 2e). The objective of the model evaluation is to demonstrate that the model is able to reproduce irrigation activities and that the irrigation scheme improves vegetation modelling and the associated surface fluxes as compared to observations. It must be noticed that the new irrigation module represents water demand for irrigation, only, and irrigation is

235 not explicitly limited by the lack of water resources. This has consequences on water conservation. Water used for irrigation is usually withdrawn from aquifers, rivers or reservoirs. These compartments are not represented in ISBA but a new module dedicated to dam/reservoirs is currently under development.

The SURFEX v8.1 version (Le Moigne et al., 2018) is used to do the simulations. Since this study focuses on irrigation, only the tile of natural and cultivated lands is simulated with ISBA, representing the evolution of soil (temperature and water profiles), vegetation (leaf-level and canopy-level photosynthesis, biomass, LAI and carbon fluxes), surface hydrology (runoff and drainage) and snow conditions. To represent the global-scale diversity of continental natural surfaces, twenty different land surface types ~~(hereafter referred to as "nature types")~~ can be used in ECOCLIMAP-SG (see Fig. S1.~~1~~ and Table S2~~1.2~~). The ISBA LSM simulations are made at a spatial resolution of 0.25° × 0.25°, over a 40-year period from 1979 to 2018. The initial values of the soil moisture and soil temperature profiles are derived from a 20-year spin-up simulation by repeating year 1979. The same initial conditions are used for all the simulations, with and without crop phenology and irrigation modelling. All land surface ~~nature~~ types are grouped into 15 patches including three irrigated ones: shrubs (orchards), C3 crops (typically wheat and rice) and C4 crops (corn). This study focuses on the results of these last two land surface ~~nature~~ types because there are hardly any irrigated orchards in Nebraska in the irrigation map described in Section 2.4.1. The dates of the irrigation season for corn are chosen in accordance with the literature (USDA and NASS, 2010) from May (emergence) to September (harvest), with a random picking of the day within those specific months. Three types of simulations are performed (Table 2): "ISBA_ref" without irrigation nor crop phenology (the benchmark), "ISBA_pheno" with only crop phenology attributes (emergence and harvest dates) and the complete "ISBA_pheno_irr" simulation with irrigation and crop phenology attributes. For the intercomparison of the simulations we select areas where the irrigation fractional coverage is larger than 50 % as determined from the irrigation map, in order to better assess the local effects of irrigation in offline simulations.

The reference ISBA_ref LAI simulations are compared with those from ISBA_pheno and ISBA_pheno_irr experiments, and with the 0.01° × 0.01° LAI satellite observations over areas in Nebraska where the vegetation is considered as C3 or C4 irrigated crops by ECOCLIMAP-SG. In addition to LAI, other variables are considered: gross primary production and land surface temperature. In order to compare the time series simulations with observations, the Pearson correlation coefficient ($r$)

and the root-mean-square difference (RMSD) scores are used. For water and carbon fluxes, they are calculated using daily values.

$$r = \frac{\sum_{i=1}^{N}(y_i-\bar{y})(x_i-\bar{x})}{\sqrt{\sum_{i=1}^{N}(y_i-\bar{y})^2 \sum_{i=1}^{N}(x_i-\bar{x})^2}}$$ (2)

where $y$ and $x$ stand for observations and model simulations, respectively, and

270 $$\bar{y} = \frac{1}{N}\sum_{i=1}^{N} y_i, \quad \bar{x} = \frac{1}{N}\sum_{i=1}^{N} x_i$$ (3)

are observation and model simulation means, respectively.

$$RMSD = \sqrt{\frac{1}{N}\sum_{i=1}^{N}(y_i - x_i)^2}$$ (4).

$N$ represents the number of observations interpolated or aggregated to the model grid. $N$ is equal to the number of model grid-cells used in the calculation of the scores.

275 The significance of $r$, $r$ differences, and RSMD differences is tested using Fisher's test, Fisher's z test, and paired sample Student's test, respectively. Significance levels of 0.01, 0.05, and 0.05 are used to reject the null hypothesis of the tests, respectively.

## 2.4 Data

### 2.4.1 Irrigation map

280 One of the main challenges of this study is to obtain an upgraded map of irrigation at the global scale, to be consistent with the resolution (300 m × 300 m) of the European Space Agency - Climate Change Initiative (ESA-CCI) land cover map used in ECOCLIMAP-SG. The 1 km × 1 km resolution global irrigation map proposed by Meier et al. (2018), based on a statistical approach and satellite data, is used. A reason to choose this product is that its development process is based (amongst other) on the ESA-
285 CCI land cover product (v1.6.1), the same as the one used to develop the ECOCLIMAP-SG vegetation map (Supplement S1).

In order to transfer the Meier irrigation map (1 km × 1 km) to ECOCLIMAP-SG (300 m × 300 m), a spatial resampling of the Meier map is performed (https://doi.org/10.5281/zenodo.7221291https://doi.org/10.5281/zenodo.6011618). A simple majority

290    rule is used by assigning to each 300 m × 300 m grid point of ECOCLIMAP-SG the irrigation status (irrigated or rainfed) of the main corresponding grid-cell of the Meier 1 km × 1 km map. An irrigation map at a spatial resolution of 300 m × 300 m is obtained, with a single vegetation type attributed to each grid cell together with the irrigation status. The main limitation of this map is that there is no information on the type of irrigation. In this study, we consider that all irrigation is of "sprinkler" type

295    as this is the most common irrigation type in the USA and in Nebraska (AQUASTAT and FAO, 2019), where the testbed area of this study is located. This entails that irrigation water is added to the precipitation forcing over the irrigated agricultural parcels.

### 2.4.2 Atmospheric forcing

The simulations presented in this study are not coupled with the atmosphere. They are driven by a
300    simulated atmospheric dataset of the European Centre for Medium-Range Weather Forecasts (ECMWF): the ERA-5 atmospheric reanalysis at 0.25° × 0.25° (Hersbach et al., 2020). This global dataset was successfully used to force the ISBA LSM in previous studies (e.g. Albergel et al., 2019, Bonan et al., 2020). Beck et al. (2019) show that the ERA-5 precipitation dataset is reasonably consistent with gauge-radar data over CONUS, except for mountainous areas. A subset of the ERA-5

305    forcing over Nebraska is used for the time period from 1979 to 2018. This period is chosen in order to encompass various validation datasets. The following atmospheric variables are used to force the ISBA LSM and are taken from ERA-5 at an hourly time step: air temperature, wind speed, air specific humidity, atmospheric pressure, shortwave and longwave downwelling radiation and precipitation (liquid and solid).

310   **2.4.3 Validation datasets**

Five observation datasets are used (Table 3) to evaluate the simulations over Nebraska: the water used for irrigation, satellite-derived Leaf Area Index (LAI), gross primary production (GPP), land surface temperature (LST), and precipitation.

      Precipitation data from the Grand Island and Lincoln weather stations (40.96°N – 98.31°W,
315   40.83°N – 96.76°W, "Gi" dot in Fig. 2e and "Li" dot in Fig. 2b, respectively) are used to evaluate the

ERA5 precipitation forcing over Nebraska. The two weather stations are within 170 km of each other and correspond to contrasting environmental conditions. While the Grand Island station is located within a densely irrigated area, the Lincoln station is located at the Lincoln airport, which is surrounded by rainfed agricultural fields.

320     The water use records are provided by the US Geological Survey (USGS) through the National Water Information System (available at https://waterdata.usgs.gov/ne/nwis/wu, last access February 2022). Every 5 years from 1985 onward, the annual raw amount of water collected for irrigation is available by county together with conveyance loss and with the surface area of the irrigated vegetation. This allows us to compute the amount of water used for irrigation per unit surface area (in mm) over the
325     specific studied zone in Nebraska (Fig. 2e). The USGS data we use cover the 1985-2019 time period. Because conveyance loss data are not available for 1995, this year is not taken into account. In order to assess the consistency of the simulated irrigation process with observations, the simulated irrigation water amount~~number of yearly irrigation events~~ on irrigated areas in Nebraska is compared with the USGS irrigation water amount estimates. Irrigation water amount is obtained from the simulated
330     number of irrigation events using the model default irrigation water amount of 30 mm per irrigation event. Values of the mean and standard deviation of the yearly irrigation amount are compared. The comparison is made for the irrigated croplands (either C3 or C4 crops) as defined using the irrigation map (Section 2.4.1) within the studied irrigated area in Nebraska (Fig. 2e).

        The simulated LAI is compared with a satellite-derived LAI product at $0.01° \times 0.01°$ spatial
335     resolution derived from SPOT-VGT and PROBA-V satellite data (up to May 2014, and after May 2014, respectively) by the European Copernicus Global Land Service (CGLS). This LAI product is described in Baret et al. (2013). We use Version 2 of this product (GEOV2). It is available every 10 days from 1999 onward. It does not cover the whole simulation time period (1979 to 2018).

        The simulated GPP is compared to an upscaled estimate of GPP available at $0.5°$ from 1980 to
340     2013, from the FLUXCOM project (Jung et al., 2017). Al-Yaari et al. (2021) show that the FLUXCOM daily evapotranspiration product can be used as a benchmark over irrigated areas. Since evapotranspiration and GPP fluxes are closely connected to each other, it can be assumed that the

FLUXCOM GPP product is also sensitive to irrigation. The FLUXCOM product is based on a global machine learning model that does not have to be locally trained. However, it seems that three flux stations in Nebraska are used in the training as their data are included in the La Thuile dataset used to build FLUXCOM (Tramontana et al. 2016). These stations are located at 45 km at the north-east of the Lincoln weather station (e.g. Suyker and Verma, 2009), in a region where irrigation is present but not dominant.

The simulated LST at 12h00 (local solar time) is compared to the LST derived from geostationary meteorological satellites by CGLS at 12h00 (local solar time). This product has a spatial resolution of 0.05° × 0.05° and is available from 2009 to 2018 (Freitas et al., 2013). It must be noticed that in the version of the model used in this study, a single composite soil-vegetation energy budget is used and the thermal effect of crop residues is not represented. This means that over croplands, the simulated LST can differ from the vegetation temperature as seen from space.

In addition to the validation datasets, corn LAI observations at the field scale for various agricultural management conditions are available in Boedhram et al. (2001).

## 3 Results

The results presented below are focused on the impacts of the crop phenology and irrigation implementation on the simulated land surface variables over Nebraska. In addition to these results, illustrations of the response to irrigation of simulated key land surface variables (SWI, LAI, GPP, evapotranspiration, LST) are shown over southwestern France and over the Hampton area in Nebraska in Supplements S2 and S3, respectively. In the case of Hampton, it can be noticed that the simulated irrigation mainly occurs in July and August (Fig. S73.1).

### 3.1 Irrigation: water use

In Fig. 3, the mean yearly irrigation amount for C3 and C4 crops for the ISBA_pheno_irr experiment is compared to the values derived from the observations from the USGS. The simulated irrigation amount presents a large interannual variability, with a minimum of 60 mm in 1993 and a maximum close to 390

mm in 2002. It must be noticed that 1993 is one of the wettest year recorded at the Lincoln weather station (https://lincolnweather.unl.edu/records/annual.asp, last access May 2022). The mean simulated value of the yearly irrigation water amount used for irrigation ($271\pm75$ mm year$^{-1}$) slightly overestimates the observed one ($264\pm65$ mm year$^{-1}$), with a difference of $+2.7\%$. This difference could be explained by the availability of the water resource, not explicitly accounted for by the model yet. The large observed irrigation amounts in 2000 and 2005, larger than 300 mm year$^{-1}$, are relatively well represented by the model. On the other hand, the observed small irrigation amount for the 2010 wet year, is overestimated by about 110 mm year$^{-1}$. In situ precipitation observations over Grand Island indicate that year 2010 is wetter than 2005 and 2000 during the growing season: 575, 508 and 277 mm from May to September, respectively. Years 2010, 2005, and 2000 are compared in Fig. S4.6. In 2010, the ERA5 precipitation bias in from July and Augustto September triggers a cumulated precipitation gap of 150 103 mm (Fig. S18a). The model responds to this water deficit by triggering irrigation at the end of the growing season, especially in August (Fig. S184.6c). On the other hand, ERA5 is unbiased at the beginning of the growing period (May-June 2010).

## 3.2 Irrigation: plant growth

Figure 4 illustrates the mean seasonal and interannual variability of LAI of irrigated crops (either C3 or C4) in the most densely irrigated part of Nebraska for areas with a fraction of irrigated crops larger than 50 % in Fig. 2e, from 1999 to 2018. Table 4 presents the peak LAI characteristics. While the satellite LAI observations present a peak at the end of July, the modelled LAI is plateauing in August (Fig. 4). The data fromFigure 2 in Boedhram et al. (2001) shows that the modelled LAI plateau in August at LAI values of about 3.7 m$^2$m$^{-2}$ is realistic for irrigated corn. The satellite LAI observations are sensitive to both rainfed and irrigated vegetation. A comparison across all vegetation types is presented in Section 3.3. In all ISBA LAI simulations, the start of the growing season corresponds to a gradual increase in LAI from the initial value of LAI = 0.30 m$^2$ m$^{-2}$ imposed to the model in winter. The observed LAI presents a smaller minimum LAI value of 0.15 m$^2$ m$^{-2}$, starts increasing in April and a value of 0.30 m$^2$ m$^{-2}$ is reached at the end of April. Then, plant growth continues at about the same low rate till the end of May. The LAI growth rate increases in June and LAI reaches a mean peak value of 4.9 ($\pm$0.8) m$^2$ m$^{-2}$ on

395  31 July (Table 4). The observed LAI then sharply decreases to reach its minimum value at about the end of September.

The ISBA_ref LAI simulations do not mirror the observed late growing season and rapid senescence. The ISBA_ref vs. observations comparison shows that without crop phenology and without irrigation the simulated LAI generally starts increasing in March. On average, a peak LAI value of 3.6

400  ($\pm$0.2) $m^2$ $m^{-2}$ is simulated by ISBA_ref on 2 July, before slowly decreasing until the end of December. The ISBA_ref growing season is much longer than observed. It starts two months before the observations and stops three months after the observations. The simulated LAI peaks one month before the observations. The simulated yearly LAI amplitude is 28 % smaller than observed.

The ISBA_pheno LAI simulation is much more consistent with the LAI observations. The

405  growing season starts in mid-May and the senescence ends at the end of September. However, the simulated peak LAI is still 30 % smaller than observed (LAI = 3.5 ($\pm$0.2) $m^2$ $m^{-2}$). The peak LAI is reached on 26 August, much later that the ISBA_ref peak LAI, and about one month after the observed peak. The sharp decrease of LAI in September results from harvests at random dates in September. Adding irrigation (ISBA_pheno_irr) does not change the general pattern of the LAI curve, but increases

410  the LAI amplitude, with a mean peak LAI value of 3.7 ($\pm$0.1) $m^2$ $m^{-2}$ on 28 August, larger (+8%) than for ISBA_pheno but still below the observation (-24%).

The interannual variability of simulated and observed LAI values is illustrated in Fig. 4b, from 2002 to 2008. The ISBA_ref LAI presents a systematic drop in summer, which is not present in the observations nor simulated by the ISBA_pheno and ISBA_pheno_irr experiments. Without the regular

415  seasonality imposed by crop phenology parameters, the model may simulate a re-growth of vegetation in autumn (e.g. in 2003), that is not present in the observations. The ISBA_pheno and ISBA_pheno_irr simulations are more consistent with the observed seasonality.

### 3.3 Impact of crop phenology and irrigation on LAI at a regional scale

This section is focused on the impact of irrigation practices for the south Nebraska zone (as defined in

420  Fig. 2e), and all land surface nature types are considered for the comparison with observations at a spatial resolution of 0.25° × 0.25°.

Figure 5a shows the seasonal mean LAI variations from 1999 to 2018. This Figure is similar to Fig. 4a but all land surface ~~nature~~ types are considered. Peak LAI characteristics are given in Table 4. They differ from the irrigated crop LAI peaks. While the observed LAI peaks at 3.8 ($\pm$1.5) $m^2$ $m^{-2}$ on 31

425 July, LAI peaks at 3.3 ($\pm$0.3) $m^2$ $m^{-2}$ on 1 July for ISBA_ref, 3.1 ($\pm$0.3) $m^2$ $m^{-2}$ on 16 July for ISBA_pheno, and 3.1 ($\pm$0.3) $m^2$ $m^{-2}$ on 16 July for ISBA_pheno_irr. Compared to irrigated crop simulations, the experiments with crop phenology (ISBA_pheno and ISBA_pheno_irr) present earlier peak LAI dates, because they include rainfed crops and natural vegetation. Emergence dates are not imposed to rainfed crops and to natural vegetation. This allows earlier leaf onset ~~rainfed vegetation~~

430 ~~affects the phenology.~~ ~~However, t~~The irrigated crop signature is visible in the second peak of the annual LAI cycle simulated by ISBA_pheno and ISBA_pheno_irr experiments at the end of August. More often than not (83 % and 88 % of the grid cells for $r$ and RMSD, respectively) the LAI score differences between ISBA_pheno_irr and ISBA_ref shown in Fig. 6 correspond to an improvement of the LAI simulation with the representation of irrigation. A month by month analysis of the scores (Fig. 7) shows

435 a significant improvement of $r$ values in June and September. The $r$ value can be increased by 30%. Lower RMSD values are observed from April to November, more frequently in May and in October. In July, RMSD differences are not significant. In April, October and November, the main cause of the reduction in RMSD values is the imposed minimum value of 0.3 $m^2$ $m^{-2}$ before the emergence (in May) and the harvest (in September). The ISBA_pheno correlation and RMSD differences with respect to

440 ISBA_ref are nearly identical to those showed for ISBA_pheno_irr in Figs. 6-7 (not shown).

## 3.4 Impact on the GPP flux

As the vegetation productivity is linked to LAI, the seasonality pattern of GPP (Fig. 5b) is comparable to the one of LAI (Fig. 5a) but the observed GPP peak (9.2 $\pm$ 2.1 g[C].$m^{-2}$.$day^{-1}$) occurs on mid-July while the observed LAI peaks on 31 July. During the plant growth period, the smallest differences

445 between all the simulations and the observations occur at about the same time as the observed GPP peak. For all simulations, a GPP plateau at a value of 9.0 $\pm$1.8 g[C] $m^{-2}$ $day^{-1}$ is reached at the beginning of July and lasts until mid-July. Finally, the simulated GPP decreases in September with a delay of about two weeks with respect to the observations.

Before July, the ISBA_ref photosynthetic activity is well in advance as compared to the observations, of about 20 days in May. This is consistent with the very large LAI values simulated by ISBA_ref in May: about 2 $m^2$ $m^{-2}$, while the mean LAI observation hardly exceeds 0.5 $m^2$ $m^{-2}$. The simulated GPP maximum (9.7 $\pm$ 2.0 g[C] $m^{-2}$ $day^{-1}$) is reached before the end of June. After a sharp decrease at the end of June, the ISBA_ref GPP decreases at a slower rate than the observations. From mid-September to the end of October, the simulated GPP is much larger than the observed GPP.

The ISBA_ref flaws are much less pronounced in ISBA_pheno and ISBA_pheno_irr experiments. In the latter simulations, the increase of the GPP occurs at about the same time as in the observations. The GPP values are systematically larger with irrigation in July and August than for other simulations. As for LAI, the GPP $r$ and RMSD scores (Fig. 6c and 6d, respectively) are better for ISBA_pheno_irr than for ISBA_ref, with an improvement on 87 % and 81 % over the domain, respectively.

### 3.5 Impact on LST

In order to evaluate the impact of irrigation on the land surface energy budget, Fig. 8 shows land surface temperature at 12h00 local time simulated by the three model configurations and derived from the CGLS product. Overall, ISBA tends to overestimate LST at noon, especially in April-May, up to 7 °C in Fig. 8a. The bias is reduced during the summer.

Due to the difficulty of observing the differences between the simulations, Fig. 8b presents differences of ISBA_pheno and ISBA_pheno_irr versus ISBA_ref. With crop phenology (with or without irrigation) the simulated LST is globally higher from April to June and from mid-September to November. The maximum difference with respect to ISBA_ref is +0.7±0.3 °C. It is observed for ISBA_pheno in September. During the summer (July and August) the new model versions tend to present lower LST values, with temperature differences close to -0.2 ± 0.1 °C in ISBA_pheno_irr. Moreover, from May to mid-September the temperature in ISBA_pheno_irr is lower than in ISBA_pheno, and this difference can reach locally -0.9°C in summer.

## 4 Discussion and perspectives

475 The results presented in Section 3 show that the new version of ISBA is able to produce a realistic mean yearly irrigation water amount (Fig. 3). It also markedly improves the LAI and GPP simulations (Figs. 5-6 and Fig. 6, respectively). On the other hand, it has a limited impact on the LST simulations and is not able to significantly reduce the strong model biases that are observed for this variable before and after the irrigation time period (Fig. 8).

480 **4.1 Could the new crop phenology and irrigation scheme be further improved?**

The crop phenology model is very simple and adding more parameters related to phenology could be a way to further improve the model performance. Integrating satellite LAI observations in ISBA using sequential data assimilation is also an option (Mucia et al., 2020). The results of our numerical experiments over Nebraska show that considering crop phenology improves the consistency of the
485 simulations with LAI and GPP observations. The corresponding correlation and RMSD scores are improved. The crop phenology parameters used to force emergence and harvest dates reduce the length of the growing season, delay spring growth and avoid a regrowth in the autumn. It seems that irrigation only plays an additive role in improving the vegetation seasonal cycle as compared to the role of including crop phenology (Section 3.3). Both crop phenology and irrigation models have shortcomings
490 and their performance are limited by difficulties in simulating processes that are not directly related to irrigation.

Firstly, the same emergence and harvest dates are imposed for all years, while in reality crop phenology may present an inter-annual variability related to climate conditions. This is particularly the case for Nebraska because the start of the growing season depends on the snowmelt and soil thawing
495 dates. These processes are represented in ISBA and crop phenology parameters could be related to snow melting and soil thawing, but this would require extensive developments to be implemented on a global scale. Moreover, the representation of the cold season processes is not perfect in ISBA (Decharme et al. 2019) and the model tends to underestimate snow depth and the length of the snow season. This could explain biases in soil temperature and LST simulations before and after the irrigation time period.

500 Figure 8 shows that LST values below the freezing level can be observed in April and that their model counterparts are about 7 °C warmer. The earlier thawing in model simulations is reflected in the much earlier leaf onset in LAI simulations. Figure 5 shows that while the observed LAI does not exceed 0.5 $m^2$ $m^{-2}$ at the end of April, the ISBA_ref LAI reaches the same value about one month earlier. The unrealistically early leaf onset is consistent with the warm model bias at the end of the cold season. This

505 shows that improving the representation of the cold season by assimilating satellite-derived or in situ snow cover fraction observations could improve the simulation of the crop growing period in this area. Also, emergence and harvest dates could be derived from the LAI observation in order to better represent the interannual variation. However, the currently used ~~empirical~~ random approach to establish the crop season provides robust results over the irrigated grid cells (Fig. 4).

510     Secondly, the irrigation itself is based on fixed parameter values such as the minimum period between two consecutive irrigations (one week) and SWI levels triggering irrigation ~~turns~~events. The simulations over the Hampton grid cell show that the first irrigation can start at quite low levels of the SWI (Fig. S7~~3.1~~), even below the second irrigation threshold of 0.55 defined in Section 2.2. Suppressing the one week constraint of irrigation ~~turns~~ events improves the simulation of the peak LAI,

515 which otherwise is rather poorly simulated (Fig. 4). However, this change triggers unrealistic large irrigation water amounts (not shown). A lack of irrigation water amount cannot explain the excessive soil water deficit. A possible explanation could be that the initial soil water storage value between the end of the cold season and the first irrigation ~~turn~~ event is withdrawn too quickly from the soil by the model. One could also challenge the quality of the ERA5 precipitation. ~~Figure S4.1 and Fig. S4.2 show~~

520 ~~that~~ ERA5 precipitation compares rather well with in situ observations and that the seasonal and inter-annual variability is fairly represented (Figs. S13 and S14). The comparison with in situ precipitation observations at the Grand Island station ~~is Supplement S4~~ shows that ERA5 tends to markedly overestimate precipitation in April, by 0.57 mm $d^{-1}$, i.e. 27 % on average from 1985 to 2018 (Fig. S15~~4.3~~). This is rather systematic: (8 years out of 10 (~~, see~~Fig. S16~~4.4~~). In July, ERA5 precipitation can

525 be much smaller than the observations, for example in 1991 and 2007 (Fig. S17~~4.5~~).

A possible limitation of using a global low-resolution reanalysis such as ERA5 is that changes to the local climatic conditions caused by irrigation may not be represented. Over Nebraska, Szilagyi and Franz (2020) show that the decadal increase in irrigated land tends to trigger a reduction in precipitation over the most densely irrigated areas, of about -10 mm per decade. The largest precipitation suppression is observed at Spring, in March, before the corn growing season, in relation to larger soil water content values. In our simulations, ISBA_pheno_irr presents larger soil moisture values than ISBA_ref in March (see Fig. S7~~3.1~~), but this is mainly due to crop phenology. The ERA5 screen-level 2 m air temperature and relative humidity are analyzed together with soil moisture by assimilating in situ observations from ground weather stations (Hersbach et al. 2020). In large irrigated areas where weather stations are present, the assimilation should be able to represent the soil moisture effect on these variables, even at coarse spatial resolution. A large-scale experiment involving ground and airborne measurements was recently performed in northeastern Spain to assess the impact of irrigation on atmospheric model simulations (Boone et al. 2021). In this context, high resolution atmospheric data from the Application of Research at the Operational Mesoscale (AROME) numerical weather forecast model are available to drive the ISBA model. AROME is run operationally at 1.3 km over western Europe. Future developments will focus on the inter-comparison of ISBA simulations at various spatial resolutions and under different conditions, as the choice of spatial resolution may affect the simulation of the smaller irrigation variabilities.

## 4.2 Are evaporation components simulated well?

All evaporation terms (plant transpiration, soil evaporation, interception) are simulated by ISBA. Under given environmental conditions, the simulated plant transpiration is not proportional to LAI. A simple canopy radiative transfer model is used to simulate the available photosynthetically active radiation (PAR) within the vegetation canopy. The response of GPP and transpiration to PAR and to LAI is controlled by this radiative transfer model. Photosynthesis and transpiration are calculated for three layers and summed to calculate canopy-level values. For large LAI values, the mean leaf-level GPP and transpiration simulations are reduced in relation to smaller vegetation transmittance to solar radiation. The impact of changes in LAI on mean leaf-level GPP and transpiration is large at

intermediate LAI values ranging from 1 to 3 $m^2m^{-2}$. It is much reduced for LAI values larger than 3 $m^2m^{-2}$. An improved version of this radiative transfer model able to represent ten canopy layers, with a more realistic response to solar zenith angle will be available in the next version of SURFEX (Delire et al. 2020). ~~The evaporation components are plotted in Fig. S3.3 and Fig. S3.4 for~~Over the Hampton irrigated area~~, in 2018. Figure S3.3 shows that~~ total evapotranspiration of ISBA_ref and ISBA_pheno_irr are quite similar (Fig. S9). On the other hand, soil evaporation and plant transpiration differ. In the ISBA_pheno_irr simulation, transpiration is reduced in spring by more than 30 %, in comparison with ISBA_ref. The lower transpiration is offset by larger soil evaporation values (Fig. S9c). As a result, total evapotranspiration does not change much. Also, ~~Fig. S3.4 shows that~~ the new crop phenology and irrigation module does not affect interception much (Fig. S10). The soil evaporation component could be overestimated because (1) the soil is too warm in relation to a poor representation of thawing or because (2) crop residues at the soil surface are not represented. Wortmann et al. (2012) show that in this area, not harvesting crop residues tends to reduce soil evaporation and increase crop yield, limit water runoff, soil erosion, and contributes to maintaining soil fertility. Suyker and Verma (2009) show that increasing surface mulch dry mass from 50 to 150 g $m^{-2}$ can decrease the non-growing season evapotranspiration by more than 20 %. The ISBA model includes a representation of litter in forests (Napoly et al. 2017) that will be generalized to low vegetation in the next version of SURFEX. Using this new capability could improve our simulations.

The use of independent evapotranspiration datasets is investigated in Supplement S3. In particular, in situ observations over an irrigated corn field (Suyker and Verma, 2009) are used. ~~Table S3.1 shows that d~~During the non-growing season, the ISBA_pheno_irr model overestimates evapotranspiration by 48 % (Table S4). ~~Table S3.2 and Fig. S3.5 show that t~~The ISBA_pheno_irr evapotranspiration peak (in June) tends to happen too early (Table S5, Fig. S11). This bias in spring could be caused by too large soil evaporation values. Mean values of near-surface wind speed are particularly large over Nebraska, especially at wintertime and springtime (Chen, 2020). This feature could exacerbate the impact of a misrepresentation of soil evaporation.

### 4.3 Is the irrigation scheme flexible enough?

In this study, sprinkling irrigation is considered. The model is able to represent other irrigation systems such as flooding irrigation but more developments are needed to limit the runoff to the irrigated plot and this options needs to be validated. The newly implemented irrigation processes, along with the new ECOCLIMAP-SG vegetation description let users choose which land surface nature type should be irrigated. Irrigation can be represented at various spatial scales, ranging from the field scale for agricultural studies to the global scale for climate studies. Model parameters can be specified using new datasets or local characteristics. For example, in this article we use a unique date for starting and ending the crop growing season with a random variability, but more accurate dates can be prescribed (varying spatially and from one vegetation type to another, or using crop calendars). Moreover, the better spatial resolution of ECOCLIMAP-SG allows the use of high resolution atmospheric forcing. This provides new opportunities for assessing the impact of irrigation on local climate and water resource conditions.

This study is mainly focused on a zone in the south of Nebraska where the irrigation density is relatively high (Fig. 2), and results could differ in other regions. Except for the fixed emergence and harvesting dates corresponding to regional crop phenology (from USDA and NASS, 2010), default values are used for all the other parameters (Section 2.4). Tests performed in southwestern France (Supplement S2) allow ensuring that the model is able to work in contrasting climate conditions.

In this study, the ISBA simulations are not coupled to the atmosphere, nor to the CTRIP river routing system. Such coupled numerical experiments can be performed thanks to the SURFEX modelling platform. However, more developments are needed in order to ensure water conservation in the hydrological system. In particular, irrigation water amounts should be consistent with the available water resource in rivers, groundwater, and dams.

### 5 Conclusions

A new uncalibrated crop phenology and irrigation scheme able to work on a global scale is implemented within the ISBA land surface model in order to improve the representation of vegetation over agricultural areas. A case study over an irrigated area in the state of Nebraska (USA) is performed

to validate the new scheme. Simple crop phenology rules represent emergence and harvesting and improve the seasonality of plant growth, while the additional water supply from the irrigation mostly impacts the peak LAI value. The model is able to produce a realistic yearly irrigation water amount and markedly improves the LAI and GPP. It is shown that model performance can be limited by processes

610 not directly related to irrigation, such as thawing or crop residues. The irrigation scheme has many possible configurations and the code is highly flexible. With this capability, ancillary data on farming practices such as emergence and harvest dates, or the amount of water per irrigation event, can be used. This flexible crop phenology and irrigation scheme can take the spatial heterogeneity of irrigation activities into account, and detect irrigation-induced impacts on Earth system simulations. Our results

615 show that crop phenology parameters modify the seasonal pattern of the simulation of LAI, soil moisture, evapotranspiration and plant carbon uptake, and that irrigation affects their magnitude. This provides the basis for further development in offline and online applications of the ISBA model.

**Code availability**

620 The ISBA land surface model is available as open source via the SURFEX modelling platform, available at https://www.umr-cnrm.fr/surfex/spip.php?article387. It is under a CECILL-C License (French equivalent to the L-GPL licence). The version developed and used for the experiment in this study is available on: https://doi.org/10.5281/zenodo.5718063. It based on the SURFEX version 8.1 (ref f70f6457). For future use, it is strongly recommended to use the newest version of ISBA, ~~from~~ within

625 the SURFEX version 9.0 (scheduled for release in 2022) ~~from~~ in which the irrigation ~~developed~~ model will be included by default. Initialization files are available on: https://doi.org/10.5281/zenodo.7221291 ~~https://doi.org/10.5281/zenodo.6011618~~.

**Author contribution**

Arsène Druel and Clément Albergel designed the experiments. Arsène Druel carried out the

630 implementation of the irrigation scheme and performed the simulations. Arsène Druel wrote the

manuscript. All co-authors participated to the analysis of the results and to the revision of the manuscript.

**Competing interests**

The authors declare that they have no conflicts of interest.

635 **Acknowledgments**

The work presented here was supported by the project URCLIM (advance on URban CLIMate services, part of ERA4CS, an ERA-NET initialised by JPI Climate with co-funding of the European Union (Grant n°690462)). The authors would like to thanks Stephanie Faroux and Marie Minvielle in charge of the SURFEX code support for technical assistance, Deborah Verfaillie for her careful reading of the
640 manuscript, and the anonymous reviewers for their helpful comments.

# References

Adegoke, J. O., Pielke, R. A., Eastman, J., Mahmood, R. and Hubbard, K. G.: Impact of Irrigation on Midsummer Surface Fluxes and Temperature under Dry Synoptic Conditions: A Regional Atmospheric Model Study of the U.S. High Plains, Mon. Weather Rev., 131(3), 556–564, https://doi.org/10.1175/1520-0493(2003)131<0556:IOIOMS>2.0.CO;2, 2003.

Al-Yaari, A., A. Ducharne, S. Tafasca, H. Mizuochi and F. Cheruy, "Influence of irrigation on the bias between ORCHIDEE and FLUXCOM evapotranspiration products," 2021 IEEE International Geoscience and Remote Sensing Symposium IGARSS, 6552-6555, https://doi.org/10.1109/IGARSS47720.2021.9554734, 2021.

AQUASTAT and FAO: Country Fact Sheet, United States of America, [online] Available from: http://www.fao.org/nr/water/aquastat/data/cf/readPdf.html?f=USA-CF_eng.pdf (Accessed 20 March 2019), 2019.

Baret, F., Weiss, M., Lacaze, R., Camacho, F., Makhmara, H., Pacholcyzk, P. and Smets, B.: GEOV1: LAI and FAPAR essential climate variables and FCOVER global time series capitalizing over existing products. Part1: Principles of development and production, Remote Sens. Environ., 137, 299–309, https://doi.org/10.1016/j.rse.2012.12.027, 2013.

Beck, H. E., Pan, M., Roy, T., Weedon, G. P., Pappenberger, F., van Dijk, A. I. J. M., Huffman, G. J., Adler, R. F., and Wood, E. F.: Daily evaluation of 26 precipitation datasets using Stage-IV gauge-radar data for the CONUS, Hydrol. Earth Syst. Sci., 23, 207–224, https://doi.org/10.5194/hess-23-207-2019, 2019.

Biemans, H., Haddeland, I., Kabat, P., Ludwig, F., Hutjes, R. W. A., Heinke, J., von Bloh, W. and Gerten, D.: Impact of reservoirs on river discharge and irrigation water supply during the 20th century, Water Resour. Res., 47(3), https://doi.org/10.1029/2009WR008929, 2011.

Boedhram, N., T. J. Arkebauer, and W. D. Batchelor: Season-long characterization of vertical distribution of leaf area in corn, Agron. J., 93, 1235–1242, https://doi.org/10.2134/agronj2001.1235, 2001.

Bonnemort, C., Bouthier, A., Deumier, J.-M., and Specty, R.: Conduire l'irrigation avec Irritel ; intérêts

et limites, La Météorologie, 14, 36-43, https://doi.org/10.4267/2042/51182, 1996.

670   Boone, A., J. Bellvert, M. Best, J. Brooke, G. Canut-Rocafort, J. Cuxart, O. Hartogensis, P. Le Moigne, J. R. Miró, J. Polcher, J. Price, P. Quintana Seguí, M. Wooster, 2021: Updates on the international Land Surface Interactions with the Atmosphere over the Iberian Semi-Arid Environment (LIAISE) Field Campaign. GEWEX News, 31(4), 16-21, available on https://www.gewex.org/gewex-content/files_mf/1640101560Q42021.pdf, last access February 2022, 2021.

675   Broadbent, A. M., Coutts, A. M., Tapper, N. J. and Demuzere, M.: The cooling effect of irrigation on urban microclimate during heatwave conditions, Urban Clim., 23, 309–329, https://doi.org/10.1016/j.uclim.2017.05.002, 2018.

Brown, T. C., Foti, R. and Ramirez, J. A.: Projected freshwater withdrawals in the United States under a changing climate, Water Resour. Res., 49(3), 1259–1276, https://doi.org/10.1002/wrcr.20076, 2013.

680   Bruinsma, J.: The Resource Outlook to 2050: By How Much Do Land, Water Use and Crop Yields Need to Increase by 2050?, Food and Agriculture Organization, Rome, Italy., 2009.

Calvet, J.-C., and Champeaux J.-L.: L'apport de la télédétection spatiale à la modélisation des surfaces continentales. La Météorologie, 108, 52-58, https://doi.org/10.37053/lameteorologie-2020-0016, 2020.

685   Calvet, J.-C., Gibelin, A.-L., Roujean, J.-L., Martin, E., Le Moigne, P., Douville, H. and Noilhan, J.: Past and future scenarios of the effect of carbon dioxide on plant growth and transpiration for three vegetation types of southwestern France, Atmospheric Chem. Phys., 8(2), 397–406, https://doi.org/10.5194/acp-8-397-2008, 2008.

Calvet, J.-C., Noilhan, J., Roujean, J.-L., Bessemoulin, P., Cabelguenne, M., Olioso, A. and Wigneron,
690   J.-P.: An interactive vegetation SVAT model tested against data from six contrasting sites, Agric. For. Meteorol., 92(2), 73–95, https://doi.org/10.1016/S0168-1923(98)00091-4, 1998.

Carrillo-Guerrero, Y., Glenn, E. P. and Hinojosa-Huerta, O.: Water budget for agricultural and aquatic ecosystems in the delta of the Colorado River, Mexico: Implications for obtaining water for the environment, Ecol. Eng., 59, 41–51, https://doi.org/10.1016/j.ecoleng.2013.04.047, 2013.

695   Chen, L.: Impacts of climate change on wind resources over North America based on NA-CORDEX,

Renewable Energy, 153, 1428-1438, https://doi.org/10.1016/j.renene.2020.02.090, 2020.

Chukalla, A. D., Krol, M. S. and Hoekstra, A. Y.: Green and blue water footprint reduction in irrigated agriculture: effect of irrigation techniques, irrigation strategies and mulching, Hydrol. Earth Syst. Sci., 19(12), 4877–4891, https://doi.org/10.5194/hess-19-4877-2015, 2015.

700 Colaizzi, P. D., Gowda, P. H., Marek, T. H. and Porter, D. O.: Irrigation in the Texas High Plains: a brief history and potential reductions in demand, Irrig. Drain., 58(3), 257–274, https://doi.org/10.1002/ird.418, 2009.

DeAngelis, A., Dominguez, F., Fan, Y., Robock, A., Kustu, M. D. and Robinson, D.: Evidence of enhanced precipitation due to irrigation over the Great Plains of the United States, J. Geophys. Res.,
705 115(D15), D15115, https://doi.org/10.1029/2010JD013892, 2010.

Decharme, B., Delire, C., Minvielle, M., Colin, J., Vergnes, J., Alias, A., Saint-Martin, D., Séférian, R., Sénési, S. and Voldoire, A.: Recent Changes in the ISBA-CTRIP Land Surface System for Use in the CNRM-CM6 Climate Model and in Global Off-Line Hydrological Applications, J. Adv. Model. Earth Syst., 11(5), 1207–1252, https://doi.org/10.1029/2018MS001545, 2019.

710 Delire, C., Séférian R., Decharme B., Alkama R., Calvet J.-C., Carrer D., Gibelin A.-L., Joetzjer E., Morel X., Rocher M., and Tzanos D.: The global land carbon cycle simulated with ISBA-CTRIP: impro-vements over the last decade, J. Adv. Mod. Earth Syst., 12, e2019MS001886, https://doi.org/10.1029/2019MS001886, 2020.

de Vrese, P., Hagemann, S. and Claussen, M.: Asian irrigation, African rain: Remote impacts of
715 irrigation, Geophys. Res. Lett., 43, 3737-3745, https://doi.org/10.1002/2016GL068146, 2016.

Döll, P., Fiedler, K. and Zhang, J.: Global-scale analysis of river flow alterations due to water withdrawals and reservoirs, Hydrol. Earth Syst. Sci., 13(12), 2413–2432, https://doi.org/10.5194/hess-13-2413-2009, 2009.

Döll, P., Hoffmann-Dobrev, H., Portmann, F. T., Siebert, S., Eicker, A., Rodell, M., Strassberg, G. and
720 Scanlon, B. R.: Impact of water withdrawals from groundwater and surface water on continental water storage variations, J. Geodyn., 59–60, 143–156, https://doi.org/10.1016/j.jog.2011.05.001, 2012.

Douglas, E. M., Niyogi, D., Frolking, S., Yeluripati, J. B., Pielke, R. A., Niyogi, N., Vörösmarty, C. J. and Mohanty, U. C.: Changes in moisture and energy fluxes due to agricultural land use and irrigation in the Indian Monsoon Belt, Geophys. Res. Lett., 33(14), L14403, https://doi.org/10.1029/2006GL026550, 2006.

Evans, R. G. and Sadler, E. J.: Methods and technologies to improve efficiency of water use, Water Resour. Res., 44(7), https://doi.org/10.1029/2007WR006200, 2008.

FAO: Food and Agriculture Organization of the United Nations: Water withdrawal and pressure on water resources, [online] Available from: http://www.fao.org/nr/water/aquastat/didyouknow/index2.stm, http://www.fao.org/nr/water/aquastat/infographics/Withdrawal_eng.pdf (Accessed 9 October 2019), 2014.

Faroux, S., Kaptué Tchuenté, A. T., Roujean, J.-L., Masson, V., Martin, E. and Le Moigne, P.: ECOCLIMAP-II/Europe: a twofold database of ecosystems and surface parameters at 1 km resolution based on satellite information for use in land surface, meteorological and climate models, Geosci. Model Dev., 6(2), 563–582, https://doi.org/10.5194/gmd-6-563-2013, 2013.

Felfelani, F., D. M. Lawrence, and Y. Pokhrel: Representing intercell lateral groundwater flow and aquifer pumping in the community land model, Water Resources Research, 56, e2020WR027531, https://doi.org/10.1029/2020WR027531, 2020.

Field, C. B., Barros, V. R., Dokken, D. J., Mach, K. J. and Mastrandrea, M. D., Eds.: Climate Change 2014 Impacts, Adaptation, and Vulnerability: Working Group II Contribution to the Fifth Assessment Report of the Intergovernmental Panel on Climate Change, Cambridge University Press, Cambridge., 2014.

Fischer, C., Montmerle, T., Berre, L., Auger, L. and Ştefănescu, S. E.: An overview of the variational assimilation in the ALADIN/France numerical weather-prediction system, Q. J. R. Meteorol. Soc., 131(613), 3477–3492, https://doi.org/10.1256/qj.05.115, 2005.

Fraiture, C. de, Wichelns, D., Rockström, J., Kemp-Benedict, E., Eriyagama, N., Gordon, L. J., Hanjra, M. A., Hoogeveen, J., Huber-Lee, A. and Karlberg, L.: Looking ahead to 2050: scenarios of

750     alternative investment approaches, in In Molden, David (Ed.). Water for food, water for life: a Comprehensive Assessment of Water Management in Agriculture., pp. 91–145, International Water Management Institute (IWMI), London, UK: Earthscan; Colombo, Sri Lanka. [online] Available from: https://hdl.handle.net/10568/36869, 2007.

Freitas, S. C., Trigo, I. F., Macedo, J., Barroso, C., Silva, R. and Perdigão, R.: Land surface temperature
755     from multiple geostationary satellites, Int. J. Remote Sens., 34(9–10), 3051–3068, https://doi.org/10.1080/01431161.2012.716925, 2013.

Gibelin, A.-L., Calvet, J.-C., Roujean, J.-L., Jarlan, L. and Los, S. O.: Ability of the land surface model ISBA-A-gs to simulate leaf area index at the global scale: Comparison with satellites products, J. Geophys. Res., 111(D18), D18102, https://doi.org/10.1029/2005JD006691, 2006.

760 Grafton, R. Q., Williams, J., Perry, C. J., Molle, F., Ringler, C., Steduto, P., Udall, B., Wheeler, S. A., Wang, Y., Garrick, D. and Allen, R. G.: The paradox of irrigation efficiency, Science, 361(6404), 748–750, https://doi.org/10.1126/science.aat9314, 2018.

Haddeland, I., Skaugen, T. and Lettenmaier, D. P.: Anthropogenic impacts on continental surface water fluxes, Geophys. Res. Lett., 33(8), L08406, https://doi.org/10.1029/2006GL026047, 2006.

765 Hanasaki, N., Inuzuka, T., Kanae, S. and Oki, T.: An estimation of global virtual water flow and sources of water withdrawal for major crops and livestock products using a global hydrological model, J. Hydrol., 384(3–4), 232–244, https://doi.org/10.1016/j.jhydrol.2009.09.028, 2010.

Harding, R. J., Blyth, E. M., Tuinenburg, O. A. and Wiltshire, A.: Land atmosphere feedbacks and their role in the water resources of the Ganges basin, Sci. Total Environ., 468–469, S85–S92,
770     https://doi.org/10.1016/j.scitotenv.2013.03.016, 2013.

Hersbach, H., Bell, B., Berrisford, P., Hirahara, S., Horányi, A., Muñoz-Sabater, J., Nicolas, J., Peubey, C., Radu, R., Schepers, D., Simmons, A., Soci, C., Abdalla, S., Abellan, X., Balsamo, G., Bechtold, P., Biavati, G., Bidlot, J., Bonavita, M., De Chiara, G., Dahlgren, P., Dee, D., Diamantakis, M., Dragani, R., Flemming, J., Forbes, R., Fuentes, M., Geer, A., Haimberger, L., Healy, S., Hogan, R.
775     J., Hólm, E., Janisková, M., Keeley, S., Laloyaux, P., Lopez, P., Lupu, C., Radnoti, G., de Rosnay, P., Rozum, I., Vamborg, F., Villaume, S., and Thépaut, J.-N.: The ERA5 Global Reanalysis, Q. J.

Roy. Meteor. Soc., 146, 730, 1999–2049, https://doi.org/10.1002/qj.3803, 2020.Hoekstra, A. Y. and Mekonnen, M. M.: The water footprint of humanity, Proc. Natl. Acad. Sci., 109(9), 3232–3237, https://doi.org/10.1073/pnas.1109936109, 2012.

780   Jägermeyr, J., Gerten, D., Heinke, J., Schaphoff, S., Kummu, M., and Lucht, W.: Water savings potentials of irrigation systems: global simulation of processes and linkages, Hydrol. Earth Syst. Sci., 19, 3073–3091, https://doi.org/10.5194/hess-19-3073-2015, 2015.

Jiang, L., Ma, E. and Deng, X.: Impacts of Irrigation on the Heat Fluxes and Near-Surface Temperature in an Inland Irrigation Area of Northern China, Energies, 7(3), 1300–1317,
785   https://doi.org/10.3390/en7031300, 2014.

Jung, M., Reichstein, M., Schwalm, C. R., Huntingford, C., Sitch, S., Ahlström, A., Arneth, A., Camps-Valls, G., Ciais, P., Friedlingstein, P., Gans, F., Ichii, K., Jain, A. K., Kato, E., Papale, D., Poulter, B., Raduly, B., Rödenbeck, C., Tramontana, G., Viovy, N., Wang, Y.-P., Weber, U., Zaehle, S. and Zeng, N.: Compensatory water effects link yearly global land CO2 sink changes to temperature,
790   Nature, 541(7638), 516–520, https://doi.org/10.1038/nature20780, 2017.

Khan, S. and Abbas, A.: Upscaling water savings from farm to irrigation system level using GIS-based agro-hydrological modelling, Irrig. Drain., 56(1), 29–42, https://doi.org/10.1002/ird.284, 2007.

Koech, R. and Langat, P.: Improving Irrigation Water Use Efficiency: A Review of Advances, Challenges and Opportunities in the Australian Context, Water, 10(12), 1771,
795   https://doi.org/10.3390/w10121771, 2018.

Kueppers, L. M., Snyder, M. A. and Sloan, L. C.: Irrigation cooling effect: Regional climate forcing by land-use change, Geophys. Res. Lett., 34(3), L03703, https://doi.org/10.1029/2006GL028679, 2007.

Lawston, P. M., Santanello, J. A., Zaitchik, B. F. and Rodell, M.: Impact of Irrigation Methods on Land Surface Model Spinup and Initialization of WRF Forecasts, J. Hydrometeorol., 16(3), 1135–1154,
800   https://doi.org/10.1175/JHM-D-14-0203.1, 2015.

Le Moigne, P. et al.: SURFEX scientific documentation - V8.1, Sci. Doc. - SURFEX [online] Available from: http://www.umr-cnrm.fr/surfex/spip.php?rubrique11 (Accessed 26 February 2018), 2018.

Lobell, D. B., Bonfils, C. J., Kueppers, L. M. and Snyder, M. A.: Irrigation cooling effect on

temperature and heat index extremes, Geophys. Res. Lett., 35(9), L09705, https://doi.org/10.1029/2008GL034145, 2008.

Masson, V., Le Moigne, P., Martin, E., Faroux, S., Alias, A., Alkama, R., Belamari, S., Barbu, A., Boone, A., Bouyssel, F., Brousseau, P., Brun, E., Calvet, J.-C., Carrer, D., Decharme, B., Delire, C., Donier, S., Essaouini, K., Gibelin, A.-L., Giordani, H., Habets, F., Jidane, M., Kerdraon, G., Kourzeneva, E., Lafaysse, M., Lafont, S., Lebeaupin Brossier, C., Lemonsu, A., Mahfouf, J.-F., Marguinaud, P., Mokhtari, M., Morin, S., Pigeon, G., Salgado, R., Seity, Y., Taillefer, F., Tanguy, G., Tulet, P., Vincendon, B., Vionnet, V. and Voldoire, A.: The SURFEXv7.2 land and ocean surface platform for coupled or offline simulation of earth surface variables and fluxes, Geosci. Model Dev., 6(4), 929–960, https://doi.org/10.5194/gmd-6-929-2013, 2013.

Meier, J., Zabel, F. and Mauser, W.: A global approach to estimate irrigated areas &ndash; a comparison between different data and statistics, Hydrol. Earth Syst. Sci., 22(2), 1119–1133, https://doi.org/10.5194/hess-22-1119-2018, 2018.

Mucia, A., Bonan, B., Zheng, Y., Albergel, C., and Calvet, J.-C.: From monitoring to forecasting land surface conditions using a land data assimilation system: Application over the contiguous United States, Remote Sens., 12, https://doi.org/10.3390/rs12122020, 2020.

Munier, S. and Decharme, B.: River network and hydro-geomorphology parametrization for global river routing modelling at 1/12° resolution, Earth Syst. Sci. Data Discuss. [preprint], https://doi.org/10.5194/essd-2021-434, in review, 2021.

Noilhan, J. and Planton, S.: A Simple Parameterization of Land Surface Processes for Meteorological Models, Mon. Weather Rev., 117(3), 536–549, https://doi.org/10.1175/1520-0493(1989)117<0536:ASPOLS>2.0.CO;2, 1989.

Ozdogan, M., Rodell, M., Beaudoing, H. K. and Toll, D. L.: Simulating the Effects of Irrigation over the United States in a Land Surface Model Based on Satellite-Derived Agricultural Data, J. Hydrometeorol., 11(1), 171–184, https://doi.org/10.1175/2009JHM1116.1, 2010.

Perry, C.: Efficient irrigation; Inefficient communication; Flawed recommendations, Irrig. Drain., 56, 367–378, 2007.

Perry, C., Steduto, P., Allen, R. G., and Burt, C. M.: Increasing productivity in irrigated agriculture: Agronomic constraints and hydrological realities, Agr. Water Manage., 96, 1517–1524, 2009.

Perry, C., Steduto, P. and Karejeh, F.: Does Improved Irrigation Technology Save Water? A Review of the Evidence, Food and Agriculture Organization, Cairo, Egypt, ISBN 978-92-5-109774-8, 2017.

835  Pfeiffer, L. and Lin, C.-Y. C.: Does efficient irrigation technology lead to reduced groundwater extraction? Empirical evidence, J. Environ. Econ. Manag., 67(2), 189–208, https://doi.org/10.1016/j.jeem.2013.12.002, 2014.

Piao, S., Ciais, P., Huang, Y., Shen, Z., Peng, S., Li, J., Zhou, L., Liu, H., Ma, Y., Ding, Y., Friedlingstein, P., Liu, C., Tan, K., Yu, Y., Zhang, T. and Fang, J.: The impacts of climate change on

840  water resources and agriculture in China, Nature, 467(7311), 43–51, https://doi.org/10.1038/nature09364, 2010.

Puma, M. J. and Cook, B. I.: Effects of irrigation on global climate during the 20th century, J. Geophys. Res., 115(D16), D16120, https://doi.org/10.1029/2010JD014122, 2010.

Rodell, M., Velicogna, I. and Famiglietti, J. S.: Satellite-based estimates of groundwater depletion in

845  India, Nature, 460(7258), 999–1002, https://doi.org/10.1038/nature08238, 2009.

Rost, S., Gerten, D., Bondeau, A., Lucht, W., Rohwer, J. and Schaphoff, S.: Agricultural green and blue water consumption and its influence on the global water system: GLOBAL WATER USE IN AGRICULTURE, Water Resour. Res., 44(9), https://doi.org/10.1029/2007WR006331, 2008.

Sacks, W. J., Cook, B. I., Buenning, N., Levis, S. and Helkowski, J. H.: Effects of global irrigation on

850  the near-surface climate, Clim. Dyn., 33(2–3), 159–175, https://doi.org/10.1007/s00382-008-0445-z, 2009.

Saeed, F., Hagemann, S. and Jacob, D.: Impact of irrigation on the South Asian summer monsoon, Geophys. Res. Lett., 36(20), L20711, https://doi.org/10.1029/2009GL040625, 2009.

Shukla, S. P., Puma, M. J. and Cook, B. I.: The response of the South Asian Summer Monsoon

855  circulation to intensified irrigation in global climate model simulations, Clim. Dyn., 42(1–2), 21–36, https://doi.org/10.1007/s00382-013-1786-9, 2014.

Siebert, S. and Döll, P.: Quantifying blue and green virtual water contents in global crop production as

well as potential production losses without irrigation, J. Hydrol., 384(3–4), 198–217, https://doi.org/10.1016/j.jhydrol.2009.07.031, 2010.

860  Siebert, S., Kummu, M., Porkka, M., Döll, P., Ramankutty, N. and Scanlon, B. R.: A global data set of the extent of irrigated land from 1900 to 2005, Hydrol. Earth Syst. Sci., 19(3), 1521–1545, https://doi.org/10.5194/hess-19-1521-2015, 2015.

Sorooshian, S., Li, J., Hsu, K. and Gao, X.: Influence of irrigation schemes used in regional climate models on evapotranspiration estimation: Results and comparative studies from California's Central
865  Valley agricultural regions: INFLUENCE OF IRRIGATION IN RCM ON ET, J. Geophys. Res. Atmospheres, 117(D6), https://doi.org/10.1029/2011JD016978, 2012.

Suyker, A. E. and Verma, S. B.: Evapotranspiration of irrigated and rainfed maize–soybean cropping systems, Agric. For. Meteorol., 149, 443-452, https://doi.org/10.1016/j.agrformet.2008.09.010, 2009.

Szilagyi, J., Franz, T.E.: Anthropogenic hydrometeorological changes at a regional scale: observed
870  irrigation–precipitation feedback (1979–2015) in Nebraska, USA, Sustain. Water Resour. Manag. 6, 10 pp., https://doi.org/10.1007/s40899-020-00368-w, 2020.

Tang, Q., Oki, T., Kanae, S. and Hu, H.: Hydrological Cycles Change in the Yellow River Basin during the Last Half of the Twentieth Century, J. Clim., 21(8), 1790–1806, https://doi.org/10.1175/2007JCLI1854.1, 2008.

875  Tramontana, G., Jung, M., Schwalm, C. R., Ichii, K., Camps-Valls, G., Ráduly, B., Reichstein, M., Arain, M. A., Cescatti, A., Kiely, G., Merbold, L., Serrano-Ortiz, P., Sickert, S., Wolf, S., and Papale, D.: Predicting carbon dioxide and energy fluxes across global FLUXNET sites with regression algorithms, Biogeosciences, 13, 4291–4313, https://doi.org/10.5194/bg-13-4291-2016, 2016.

880  United Nations, Department of Economic and Social Affairs and Population Division: World population prospects Data booklet, 2019 revision Data booklet, 2019 revision., 2019.

USDA and NASS: Farm and ranch irrigation (2008), Special Studies in 2007 Census Publications, United States Department of Agriculture, National Agricultural Statistics Service, AC-07-SS-1. [online]                              Available                              from:

885   https://www.nass.usda.gov/Publications/AgCensus/2007/Online_Highlights/Farm_and_Ranch_Irriga
tion_Survey/fris08.pdf, 2009.

USDA and NASS: Field Crops, Usual Planting and Harvesting Dates, United States Department of
Agriculture - National Agricultural Statistics Service. [online] Available from:
https://downloads.usda.library.cornell.edu/usda-
890   esmis/files/vm40xr56k/dv13zw65p/w9505297d/planting-10-29-2010.pdf (Accessed 4 July 2019),
2010.

Verburg, P. H., Dearing, J. A., Dyke, J. G., Leeuw, S. van der, Seitzinger, S., Steffen, W. and Syvitski,
J.: Methods and approaches to modelling the Anthropocene, Glob. Environ. Change, 39, 328–340,
https://doi.org/10.1016/j.gloenvcha.2015.08.007, 2016.

895 Voirin-Morel, S.: Hydrographical modelling at a regional scale : application to the Adour-Garonne
basin, Toulouse 3., 2003.

Voldoire, A., Decharme, B., Pianezze, J., Lebeaupin Brossier, C., Sevault, F., Seyfried, L., Garnier, V.,
Bielli, S., Valcke, S., Alias, A., Accensi, M., Ardhuin, F., Bouin, M.-N., Ducrocq, V., Faroux, S.,
Giordani, H., Léger, F., Marsaleix, P., Rainaud, R., Redelsperger, J.-L., Richard, E. and Riette, S.:
900   SURFEX v8.0 interface with OASIS3-MCT to couple atmosphere with hydrology, ocean, waves and
sea-ice models, from coastal to global scales, Geosci. Model Dev., 10(11), 4207–4227,
https://doi.org/10.5194/gmd-10-4207-2017, 2017.

Yin, Z., Wang, X.H., Ottlé, C., Zhou, F., Guimberteau, M., Polcher, J., Peng, S.S., Piao, S.L., Li, L., Bo,
Y., Chen, X.L., Zhou, X.D., Kim, H., Ciais, P.: Improvement of the irrigation scheme in the
905   ORCHIDEE land surface model and impacts of irrigation on regional water budgets over China. J.
Adv. Model. Earth Syst. 12, 1–20. https://doi.org/10.1029/2019MS001770, 2020.

Zaitchik, B. F., Evans, J. and Smith, R. B.: MODIS-Derived Boundary Conditions for a Mesoscale
Climate Model: Application to Irrigated Agriculture in the Euphrates Basin, Mon. Weather Rev.,
133(6), 1727–1743, https://doi.org/10.1175/MWR2947.1, 2005.

910 Zhang, G., D. Shen, B. Ming, R. Xie, X. Jin, C. Liu, P. Hou, J. Xue, J. Chen, W. Zhang, W. Liu, K.
Wang, S. Li: Using irrigation intervals to optimize water-use efficiency and maize yield in Xinjiang,

northwest China, The Crop J., 7, 322-334, https://doi.org/10.1016/j.cj.2018.10.008, 2019.

Zhang, Z., M. Barlage, F. Chen, Y. Li, W. Helgason, X. Xu, X. Liu, and Z. Li: Joint modeling of crop and irrigation in the central United States using the Noah-MP land surface model. Journal of
915      Advances in Modeling Earth Systems, 12, e2020MS002159, https://doi.org/10.1029/2020MS002159, 2020.

920

**Table 1 – Irrigation parameters.**

| Symbol | Definition | Range | Default value (this study) |
|---|---|---|---|
| $I_T$ | Irrigation type | Sprinkler, flood, and drip irrigation | sprinkler |
| $I_{NT}$ | Irrigated ~~nature~~ land surface type | All 20 land surface types (Fig. S1) | C3 crops, C4 crops, shrubs |
| $I_W$ | Water amount per irrigation ~~water turn~~ event | 0 mm or more | 30 mm |
| $I_D$ | Irrigation ~~water turn~~ event duration | 0.25 hour or more | 8 hours |
| $SWI_1$ | S~~oil wetness index~~WI threshold for triggering the first irrigation event ~~water turn~~ | 0 to 1 | 0.70 |
| $SWI_2$ | Soil wetness index~~SWI~~ threshold for triggering the second irrigation event~~water turn~~ | 0 to 1 | 0.55 |
| $SWI_3$ | Soil wetness index~~SWI~~ threshold for triggering the third irrigation event~~water turn~~ | 0 to 1 | 0.40 |
| $SWI_{4+i}$ | Soil wetness index~~SWI~~ threshold for triggering the following irrigation events ~~water turns~~ (i, integer > 0) | 0 to 1 | 0.25 |
| $\Delta t_{Wn}$ | Minimum time ~~lapse~~ interval between two irrigation events ~~water turns~~ (irrigation interval) | 0 days (e.g. drip irrigation) or more | 7 days ~~(0 days for drip irrigation)~~ |
| $\Delta t_{WH}$ | Minimum time ~~lapse~~ interval between the last irrigation event~~water turn~~ and the harvest | 0 to 365 days | 15 days |
| $t_E$ | Emergence date | 1 January to 31 December | 15 May (± 15 days) |
| $t_H$ | Harvest date | 1 January to 31 December After emergence date | 15 September (± 15 days) |

925

**Table 2** – **Main set up of the three 40-year evaluation experiments driven by ERA-5 atmospheric variables over Nebraska. Crop phenology is defined by emergence and harvest dates, while irrigation corresponds to additional water supply.**

| Experiment | Crop phenology | Irrigation | Forcing | Spinup time | Simulation time period |
|---|---|---|---|---|---|
| ISBA_ref | no | no | ERA-5 0.25° × 0.25° | 20 years | 1979-2018 |
| ISBA_pheno | YES | no | | | |
| ISBA_pheno_irr | YES | YES | | | |

930

**Table 3 – Evaluation datasets.**

| Observations | Source | Reference | Spatial resolution | Sampling time | Time period | Number over the time period |
|---|---|---|---|---|---|---|
| Water used for irrigation | USGS | https://waterdata.usgs.gov/ne/nwis/wu | County | 5 years | 1985-2015 | 6 |
| LAI | CGLS | Baret et al. (2013) | 0.01° | 10 days | 1999-2018 | 720 |
| GPP | FLUXCOM | Jung et al. (2017) | 0.25° | 1 month | 1980-2013 | 408 |
| Land surface temperature at 12h | CGLS | Freitas et al. (2013) | 0.05° | 1 day | 2009-2018 | 439 or more (see Fig. S123.6) |
| In situ precipitation | University of Nebraska-Lincoln | http://climod.unl.edu/ | local | 1 month | 1985-2018 | 408 |

**Table 4 – Observed and simulated mean LAI peak characteristics over Nebraska for the 1999-2018 time period for irrigated crops (see Fig. 4) and all ~~vegetation~~ land surface types (see Fig. 5).**

| Vegetation types | LAI source | Peak LAI (m² m⁻²) | Peak LAI date |
|---|---|---|---|
| Irrigated c~~C~~rops | Satellite observations | 4.9 (±0.8) | 31 July |
| | Boedhram et al. 2001 (*) | 3.6 to 4.0 | 12 July to 19 August 1994 |
| | Boedhram et al. 2001 (*) | 3.5 | 2 August to 23 August 1995 |
| | ISBA_ref | 3.6 (±0.2) | 2 July |
| | ISBA_pheno | 3.5 (±0.2) | 26 August |
| | ISBA_pheno_irr | 3.7 (±0.1) | 28 August |
| All land surface types | Satellite observations | 3.8 (±1.5) | 31 July |
| | ISBA_ref | 3.3 (±0.3) | 1 July |
| | ISBA_pheno | 3.1 (±0.3) | 16 July |
| | ISBA_pheno_irr | 3.1 (±0.3) | 16 July |

940    (*) Boedhram et al. (2001) data are for fertilized irrigated corn in 1994 and 1995

945
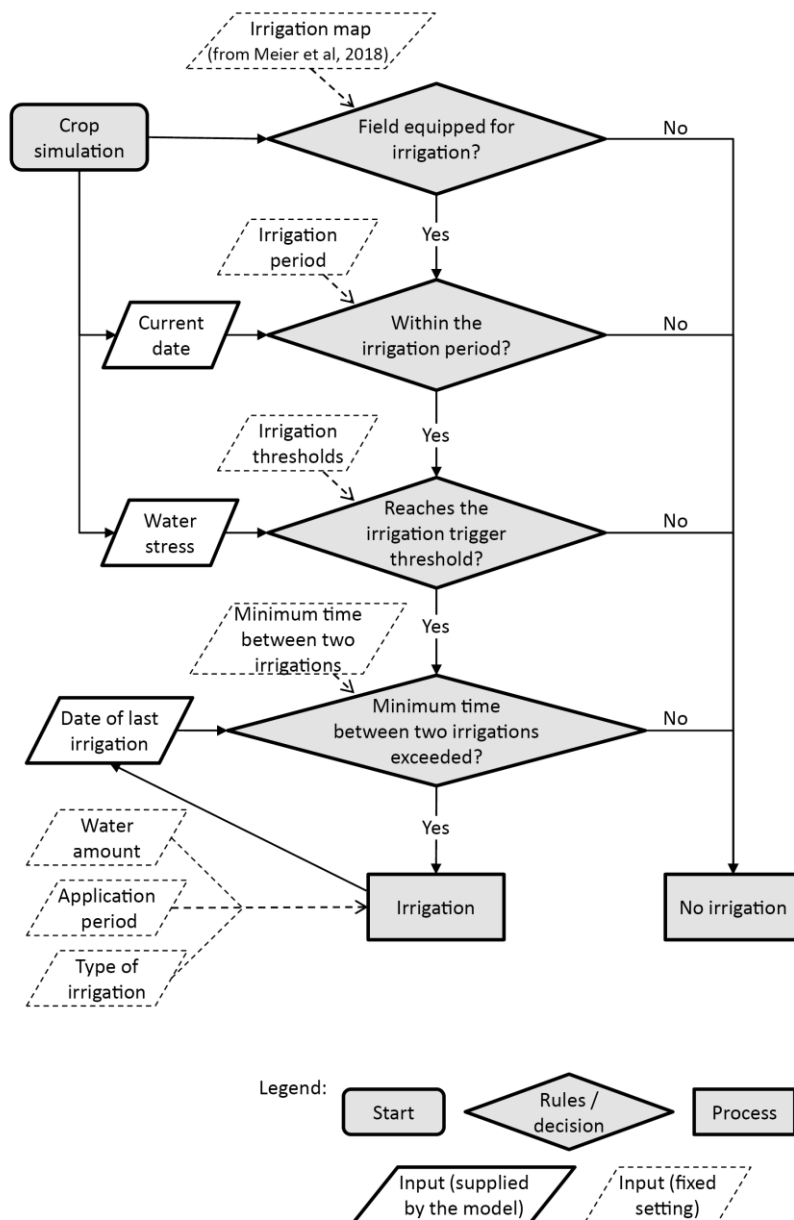
**Figure 1 – Irrigation decision tree model.**
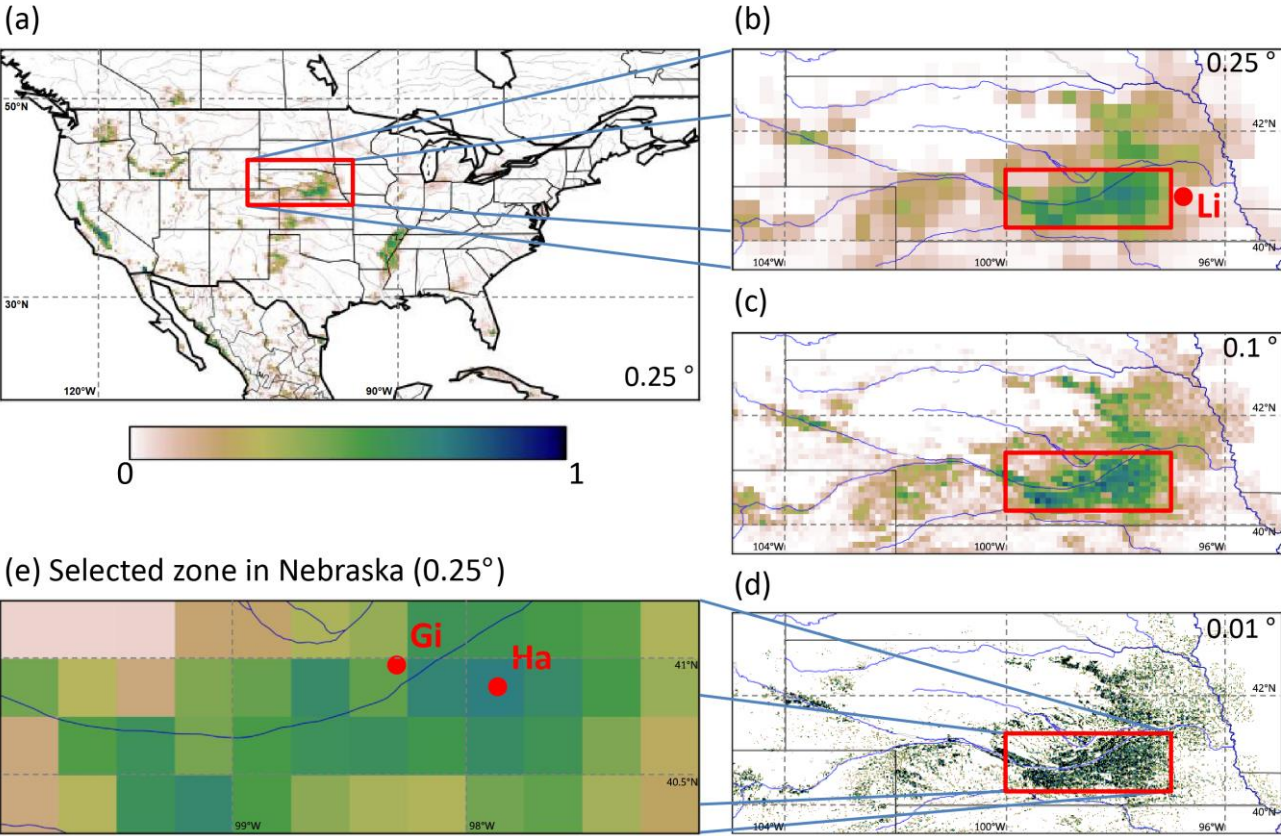
**Figure 2 – Irrigation fractional coverage derived from Meier et al. (2018) over (a) the Continental United State (CONUS), (b, c, d, e) Nebraska: at (b) 0.25°×0.25°, (c) 0.1°×0.1°, (d) 0.01°×0.01° spatial resolutions, and (e) over the selected zone in southern Nebraska considered in this study (100-97°W, 40.25-41.25°N). The red boxes show the location of the different zooms. The "Li", "Gi" and "Ha" red dots correspond to the Lincoln weather station, Grand Island weather station, and Hampton irrigated area, respectively.**
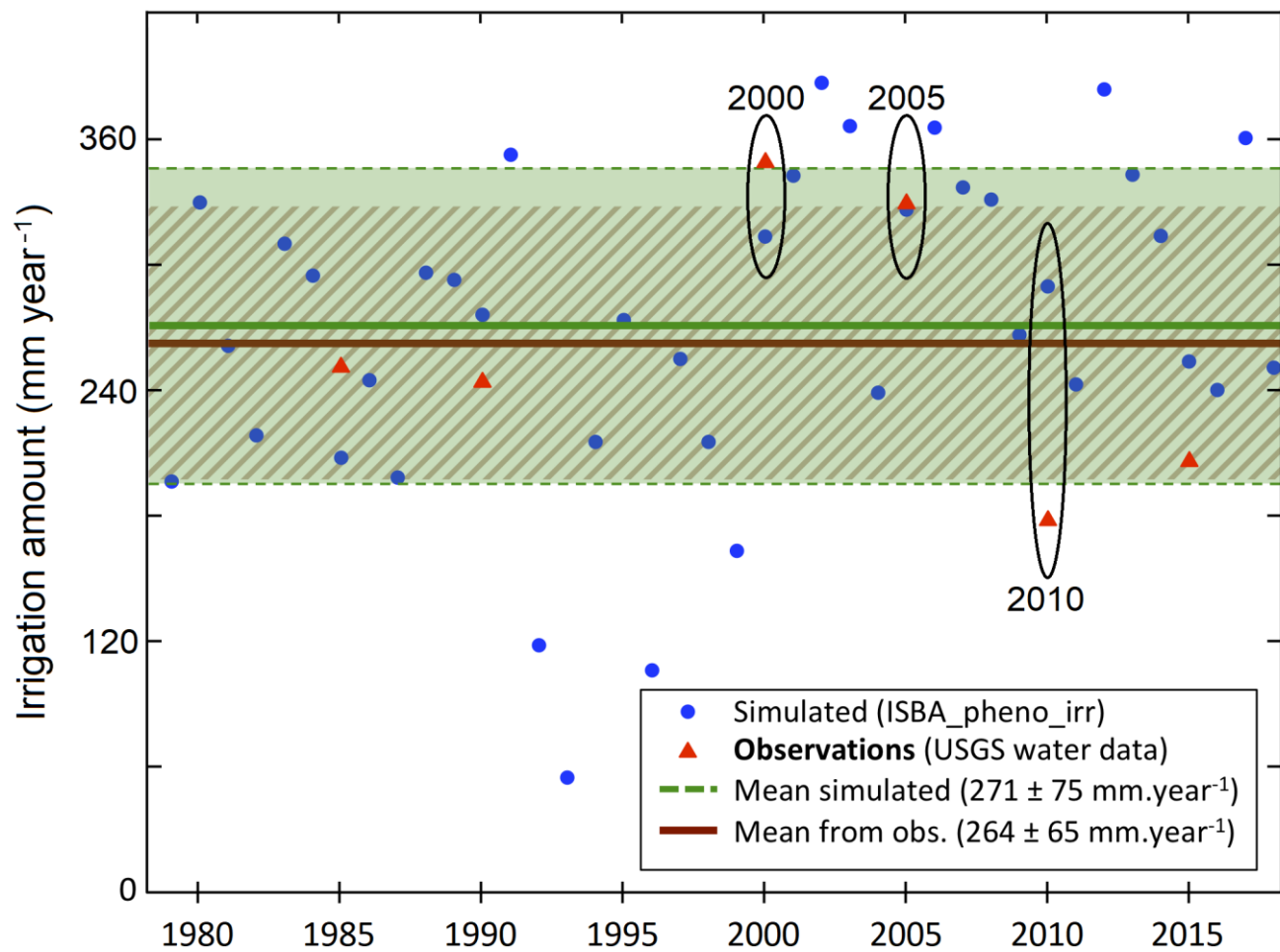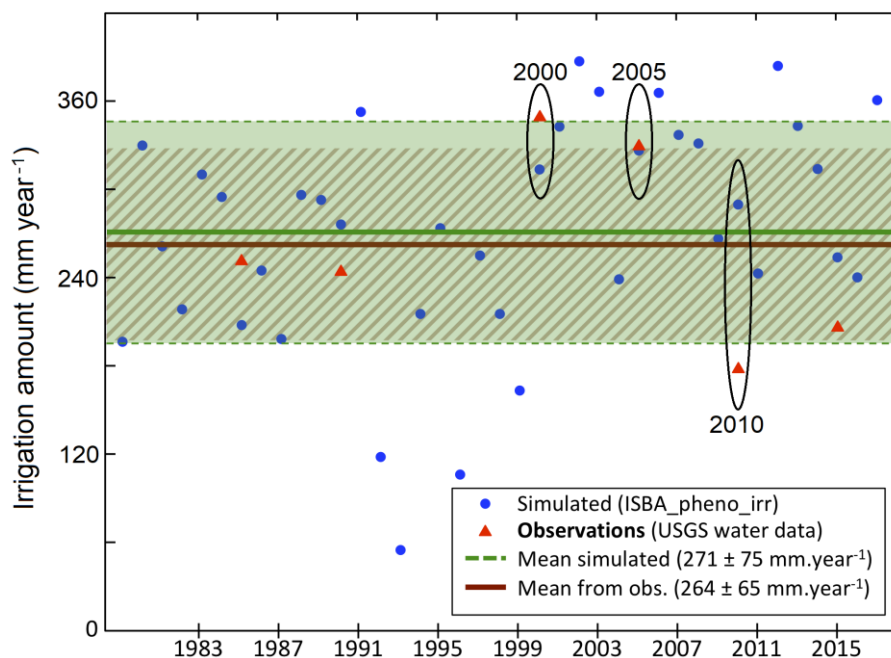
**Figure 3** – **Yearly cumulated irrigation amounts simulated by the model for the studied area in Nebraska from 1979 to 2018 (blue dots). The six USGS observations from 1985 to 201~~5~~8 are shown (red triangles). The mean and standard deviation of the yearly values are shown for the model (green solid and dashed lines, respectively), and for the USGS data (brown lines). The 2000 and 2005 dry years are indicated, together with the 2010 wet year.**
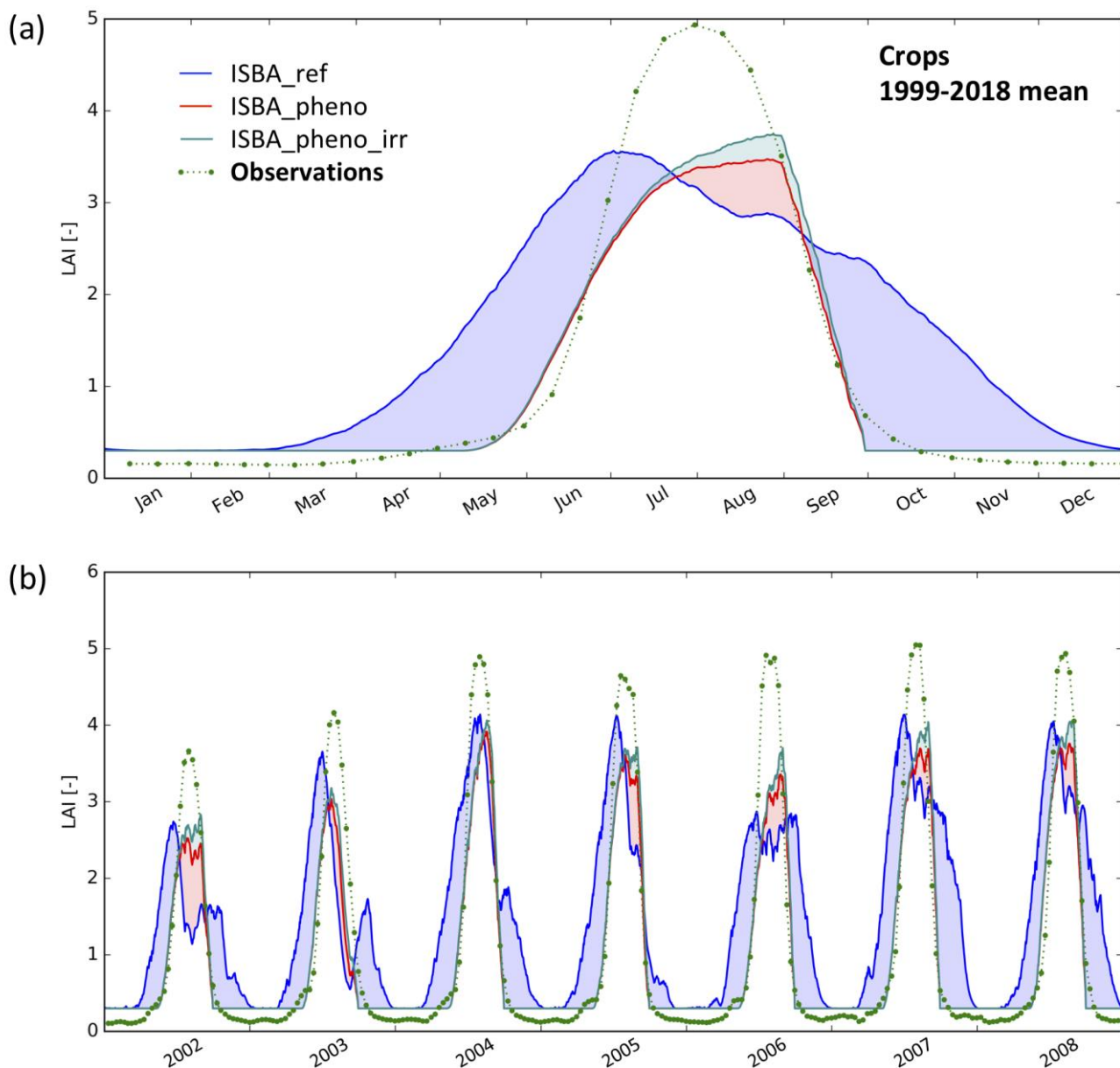
**Figure 4 – LAI (m² m⁻²) of irrigated crops (C3 or C4) in the most densely irrigated part of Nebraska (Fig. 2e): (a) seasonal variation for the time period from 1999 to 2018, (b) daily time series from 2002 to 2008. Simulated LAI is shown for the irrigated fraction, from the reference simulation (ISBA_ref, blue line), and from the simulations with only agricultural practices and with agricultural practices and irrigation (ISBA_pheno, red line, and ISBA_pheno_irr, cyan line, respectively). Satellite-derived LAI observations (green dots) are for areas where the fraction of C3 or C4 irrigated crops is larger than 50 %.**
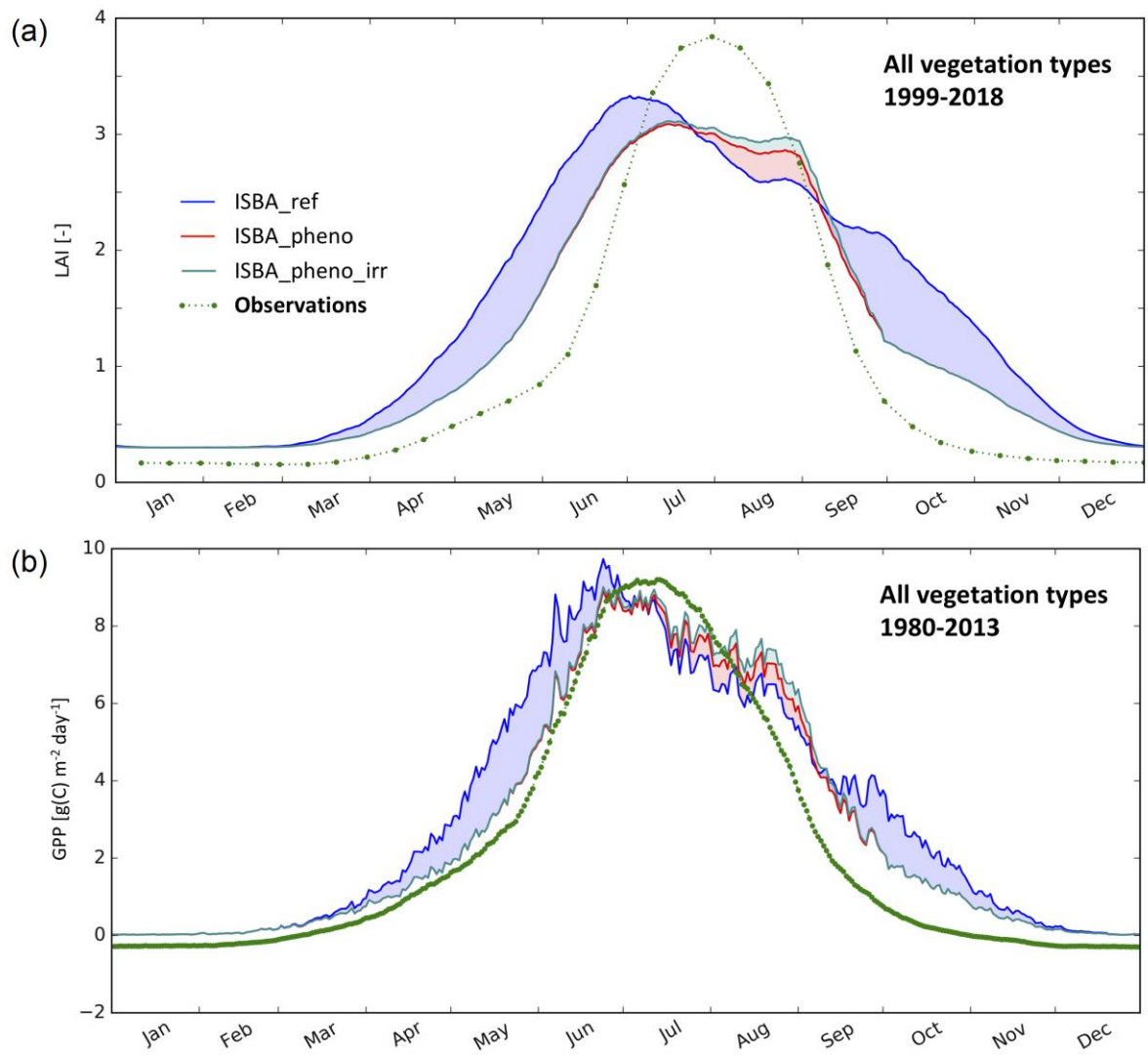
**Figure 5 – Simulated vs. observed LAI and GPP of all vegetation types, in the most densely irrigated part of Nebraska (Fig. 2e): (a) seasonal variation of mean LAI (m²m⁻²) from 1999 to 2018, (b) seasonal variation of mean GPP (gC m⁻² d⁻¹) 1980 to 2013. ISBA_ref, ISBA_pheno, ISBA_pheno_irr simulations are represented by blue, red, and cyan lines, and satellite-derived observations by green dots.**
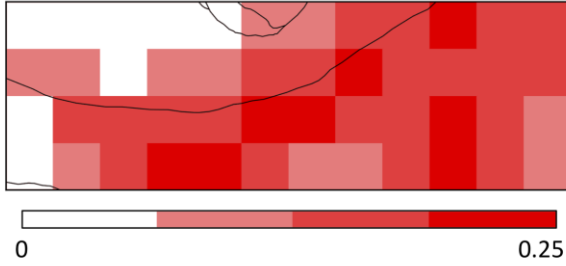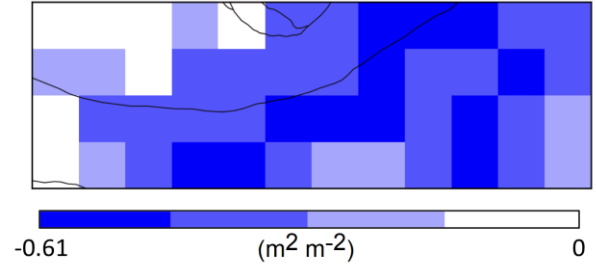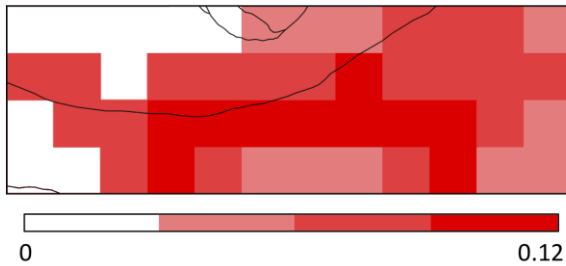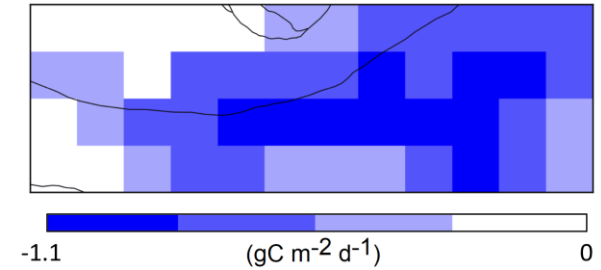
990

**Figure 6 – Simulated vs. observed LAI and GPP of all vegetation types, in the most densely irrigated part of Nebraska (Fig. 2e): (a, c) temporal correlation and (b, d) RMSD score difference maps of (a, b) LAI, and (c, d) GPP. White is used to mask non-significant score difference values.**

995
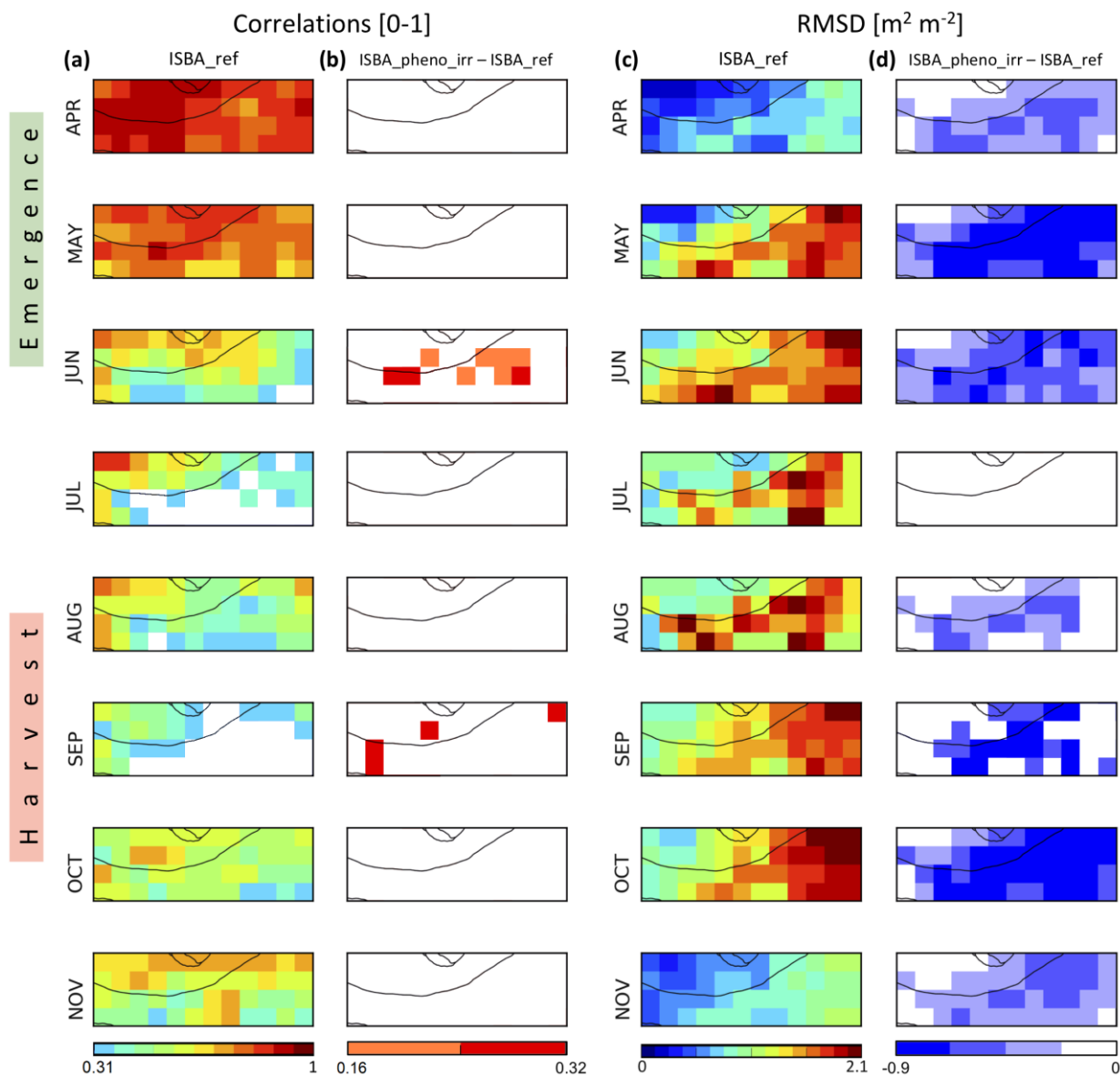
**Figure 7 – Comparison of simulated LAI with CGLS LAI observations in the most densely irrigated part of Nebraska (Fig. 2e) from 1999 to 2018 during the vegetation growing and senescence time period from April to November. Monthly temporal correlation (a, b) and RMSD (c, d) maps are shown for the reference simulation without a representation of irrigation ISBA_ref (a, c). The added value of the ISBA_pheno_irr simulation with respect to ISBA-ref is shown through score difference maps (b, d). White is used to mask non-significant correlation and score difference values.**

1005
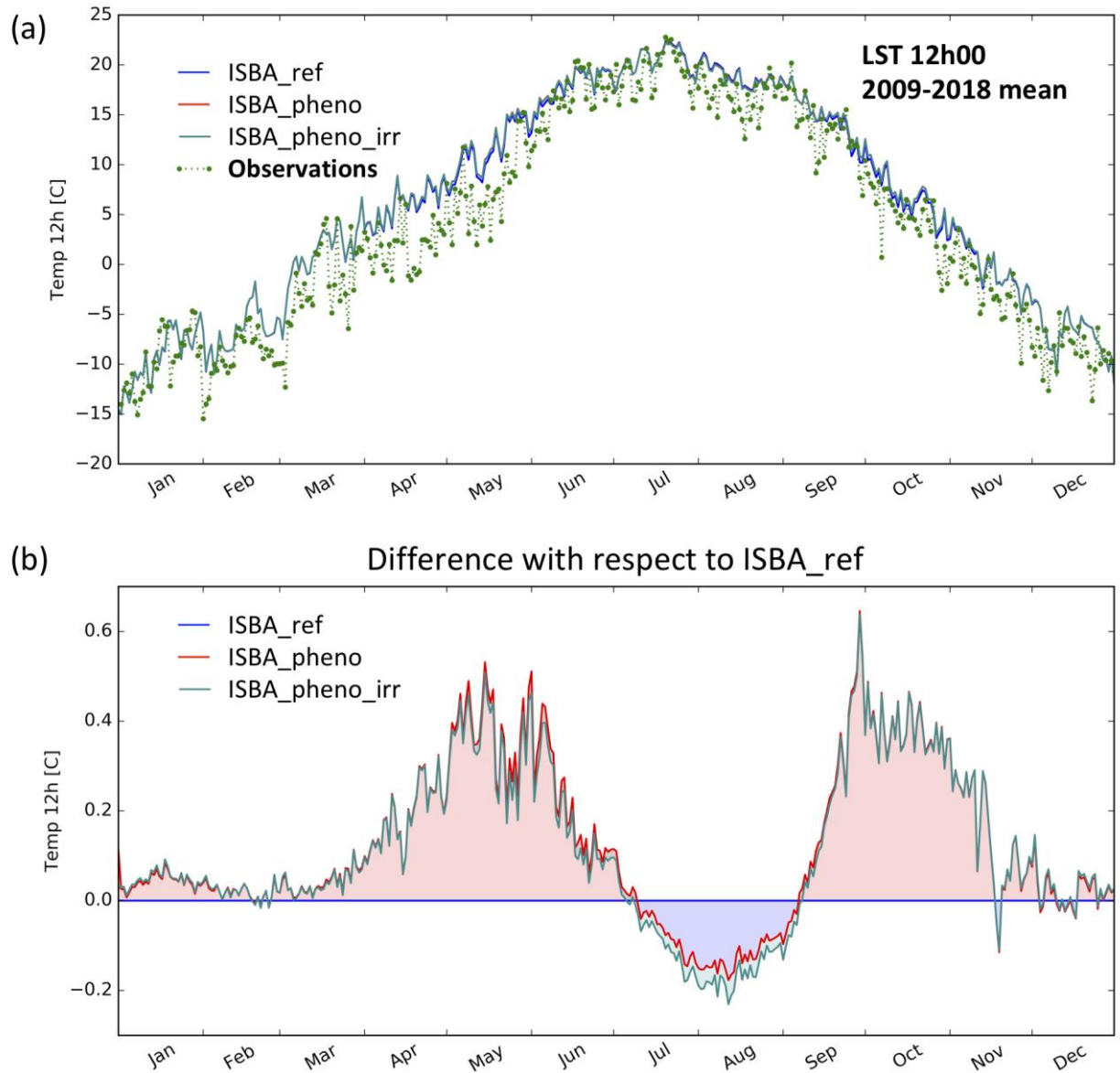
**Figure 8 – Seasonal variation of surface temperature daily values at 12:00 local time (degree C) in the most densely irrigated part of Nebraska (Fig. 2e) from 2009 to 2018 (a) as derived from the reference simulation ISBA_ref (blue line), ISBA_pheno (red line), ISBA_pheno_irr (cyan) and the CGLS product (green dotted line). The surface temperature differences at 12:00 local time (b) of**
1010 **ISBA_pheno_irr and ISBA_pheno simulations with respect to the ISBA-ref simulations are shown.**